Sedimentary record from the Canada Basin, Arctic Ocean: implications for late to middle Pleistocene glacial history

Linsen Dong[1,2], Yanguang Liu[1,2], Xuefa Shi[1,2,*], Leonid Polyak[3], Yuanhui Huang[1,2], Xisheng Fang[1], Jianxing Liu[1,2], Jianjun Zou[1,2], Kunshan Wang[1,2], Fuqiang Sun[1], Xuchen Wang[4].

[1]Key Laboratory of Marine Sedimentology and Environmental Geology, First Institute of Oceanography, State Oceanic Administration, Qingdao 266061, China

[2]Laboratory for Marine Geology, Qingdao National Laboratory for Marine Science and Technology, Qingdao, 266 061, China

[3]Byrd Polar and Climate Research Center, The Ohio State University, 43210, USA

[4]Key Laboratory of Marine Chemistry Theory and Technology, Ocean University of China, Qingdao 266100, China

*Corresponding author.Tel./fax: +86 532 88967491

E-mail address:xfshi@fio.org.cn(X.Shi)

Abstract: Sediment core ARC4–BN05 collected from the Canada Basin, Arctic Ocean, covers the late to middle Quaternary (Marine Isotope Stages (MIS) 1-15, ca. 0.5-0.6 Ma) as estimated by correlation to earlier proposed Arctic Ocean stratigraphies and AMS ^{14}C dating of the youngest sediments. Detailed examination of clay and bulk mineralogy along with grain size, content of Ca and Mn, and planktonic foraminiferal numbers in core ARC4–BN05 provides important new

information about sedimentary environments and provenance. We use increased contents of coarse debris as an indicator of glacier collapse events at the margins of the western Arctic Ocean, and identify the provenance of these events from mineralogical composition. Notably, peaks of dolomite debris, including large dropstones, track the Laurentide Ice Sheet (LIS) discharge events to the Arctic Ocean. Major LIS inputs occurred during the stratigraphic intervals estimated as MIS 3, intra-MIS 5 and 7 events, MIS 8, and MIS 10. Inputs from the East Siberian Ice Sheet (ESIS) are inferred from peaks of smectite, kaolinite, and chlorite associated with coarse sediment. Major ESIS sedimentary events occurred in the intervals estimated as MIS 4, MIS 6 and MIS 12. Differences in LIS vs. ESIS inputs can be explained by ice-sheet configurations at different sea levels, sediment delivery mechanisms (iceberg rafting, suspension plumes, and debris flows), and surface circulation. A long-term change in the pattern of sediment inputs, with an apparent step change near the estimated MIS 7/8 boundary (ca. 0.25 Ma), presumably indicates an overall glacial expansion at the western Arctic margins, especially in North America.

Keywords: Sediment core, Pleistocene, western Arctic Ocean, clay minerals, bulk minerals, sediment provenance, Laurentide Ice Sheet, East Siberian Ice Sheet

1. Introduction

The advances and decays of continental ice sheets play a significant role in the alteration of global climatic system, such as changing atmospheric circulations, creating large area albedo anomalies and regulating the global sea level fluctuations

(Clark et al., 1990). Reconstruction of the history of ice sheets is therefore important not only for a better understanding of feedbacks of the future climate change and its impact on regional climates, but also for getting insights into the mechanisms of abrupt climate change.

Studies of Pleistocene glaciations around the Arctic Ocean dealt mostly with the late Quaternary history of the Eurasian Ice Sheet during Marine Isotope Stages (MIS) 1–6 (e.g., Svendsen et al., 2004; Larsen et al., 2006) or the Laurentide Ice Sheet (LIS) with a special attention to the Last Glacial Maximum (LGM) (e.g. Dyke et al., 2002; England et al., 2009). In addition to terrestrial data, studies of sediment cores from the Arctic Ocean are critical for comprehending the history of glacial advances and retreats (e.g., Polyak et al., 2004; 2009; Spielhagen et al., 2004; Stein et al., 2012; Kaparulina et al., 2015). However, the long-term history of circum-Arctic glaciations is still poorly understood, especially with respect to the western Arctic including the North America and East Siberia. While a major impact of the North American ice sheets on circulation and depositional environments in the Arctic Ocean is indicated by various marine and terrestrial data (e.g., Phillips and Grantz, 2001; Stokes et al., 2005), the East Siberian Ice Sheet (ESIS) remained largely hypothetical until recently. Some terrestrial and seafloor mapping data now provide evidence for the existence of considerable ice masses on the East Siberian margin (Basilyan et al., 2010; Niessen et al., 2013; Dove et al., 2014), but the timing and extent of these glaciations is virtually unknown. Marine sedimentary records from the Arctic Ocean adjacent to the East Siberian margin could add valuable information to this intriguing paleoglaciological

problem.

In this paper, we present a multiproxy study of glacial-interglacial changes during the late to middle Pleistocene based on sediment core ARC4-BN05 from the Canada Basin north of the Chukchi Plateau and east of the Mendeleev Ridge. This location can be affected by the two main Arctic Ocean circulation systems, the Beaufort Gyre and the Transpolar Drift, which carry sea ice, icebergs, and sediment discharge from the North America and Siberia, respectively. As this circulation along with sedimentary environments and sources varied greatly during the Pleistocene climate cycles, resulting variations in sediment delivery and deposition make for a valuable paleoclimatic record for the western Arctic. Biogenic proxies (such as foraminifers) have uneven and overall limited distribution in Arctic Ocean sediments, while the terrigenous component provides a more consistent material for paleoceanographic studies (e.g. Stein, 2008; Polyak et al., 2009). As sediments in the Arctic Ocean are primarily transported by sea ice and/or icebergs during glacial events, sediment composition yields important information not only on the provenance and transport pathways, but also on the attendant glacial and paleoclimatic history (e.g. Spielhagen et al., 1997; Vogt et al., 2001; Knies et al., 2001). By using clay and bulk mineralogy, along with grain size and the content of major elements Ca and Mn, we reconstruct depositional environments and sediment provenance to provide clues to the history of western Arctic ice sheets and their interaction with the Arctic Ocean.

2. Regional background

The Arctic Ocean is surrounded by land masses composed of an assortment of lithologies and situated in a variety of climatic, tectonic, and physiographic settings. Figure 1 depicts a schematic geological map showing the main terrains and associated lithologies (Fagel et al., 2014). The West Siberian Basin, East Siberian platform and Verkhoyansk-Chukotka provinces of the Eurasian continent are mainly composed of terrigenous sediment (Fagel et al., 2014). The Siberian (Putorana) traps constitute one of the largest flood basalts in the world (Sharma et al., 1992). The western Okhotsk-Chukotsk volcanic belt contains acidic to intermediate rocks, whereas intermediate to basic rocks are more characteristic of the eastern side (Viscosi-Shirley et al., 2003). The Kara Plate and the Taymyr foldbelt, as well as the Ural and Novaya Zemlya foldbelt are mainly composed of intrusive and metamoprhic rocks (Fagel et al., 2014).

The geology of outcropping terraines of Alaska mainly includes Canadian-Alaskan Cordillera, Brooks Range, and part of the Northern-American platform containing mostly intrusive, metamoprhic, and some clastic rocks (Fagel et al., 2014). The outcrops of the Canadian Arctic Archipelago are mainly composed of carbonate and clastic rocks (Phillips and Grantz, 2001; Fagel et al., 2014), whereas intrusive and clastic rocks are mostly characteristic for Greenland (Fagel et al., 2014).

Dissolved and suspended matter is transported to the Arctic Ocean by voluminous rivers, with the Lena and Mackenzie Rivers being the largest on the Siberian and North American side, respectively. The transported material is further

distributed across the Arctic Ocean in water and/or ice by currents. The two main surface, wind-driven circulation systems are the clockwise Beaufort Gyre (BG) in the western Arctic and the Transpolar Drift (TPD) that carries water and ice from the Siberian margin to the Norwegian-Greenland Sea (e.g., Rudels, 2009). The strength and trajectories of these current systems may vary depending on changes in atmospheric pressure fields known as the Arctic Oscillation (Rigor et al., 2002).

Sedimentation in the Arctic Ocean is strongly controlled by sea ice that acts as sediment carrier, but can also suppress sediment deposition under thick and persistent ice cover (Darby et al., 2006; Polyak et al., 2009). During glacial/deglacial events, multiple icebergs discharged into the Arctic Ocean from the termini of marine-based ice sheets and strongly affected sediment dispersal and deposition (e.g., Spielhagen et al., 2004; Polyak et al., 2009). Fine-grained sediments can also be transported by subsurface and deep-water currents, such as the Atlantic water (Winkler et al., 2002), but their role in the overall Arctic Ocean sedimentation is not well understood.

3. Materials and methods

Gravity core ARC4-BN05 (referred hereafter as BN05) was collected from the Canada Basin in the vicinity of the Mendeleev Ridge (80° 29.04′ N, 161° 27.90′ W, 3156 m water depth) (Fig. 1) on the fourth Chinese National Arctic Research Expedition (CHINARE-Ⅳ) in 2009. The BN05 site was chosen in a close proximity to earlier investigated cores FL224 and PS72/392-5 (Stein et al., 2010a) to enable robust correlation with the established stratigraphies. A total of 119 samples were

taken at 2-cm intervals over the 238-cm BN05 length, and kept frozen until analyzed.

For age constraint within the radiocarbon range, Accelerator Mass Spectrometry ^{14}C dating was performed on 1000–1200 tests of planktic foraminifers *Neogloboquadrina pachyderma* sin. (＞63 μ m) from core depths at 4-6, 8-10, 18-20 and 22-24 cm, using the NOSAMS facilities at Woods Hole Oceanographic Institution.

For grain-size analysis, ~2-g sediment samples were successively treated with 15 ml 15% H_2O_2, 5 ml 3mol/L HCl, and 20 ml 1mol/L Na_2CO_3 for removing organic matter, biogenic carbonates, and biogenic silica, respectively. Grain size measurements in the range of 0.02 to 2000 μm were performed on a Malvern Mastersize laser particle sizer (Mastersizer 2000) in the First Institute of Oceanography, SOA, China.

Coarse sediment >63 μm was sieved from ~10–15 g samples and counted under the microscope for foraminiferal and mineral grain numbers.

Elemental abundances, given in peak area (counts per second, cps), were obtained at 1 cm resolution using the Itrax XRF core scanner at the Polar Research Institute of China, setting at 20 s count times, 10 kV X-ray voltage and an X-ray current of 20 mA. The obtained count values are used as estimates of relative concentrations. In addition, concentrations of major elements, such as Ca and Mn, were determined on point samples by ICP-OES (iCAP6300) at the First Institute of Oceanography, SOA, China, following the standard procedures.

Color reflectance was measured using a hand-held Minolta CM-2002

154 spectrofotometer at 1 cm intervals. Only the grayscale lightness index (L*) is used in
155 this paper.

156 A total of 60 2-cm-thick samples were collected at 4-cm interval for
157 paleomagnetic measurements performed at the Paleomagnetism and Geochronology
158 Laboratory of the Institute of Geology and Geophysics, Chinese Academy of Science.
159 Magnetic susceptibility was measured using the KLY-4s Kappabridge instrument.
160 Subsequently, stepwise alternating field (AF) demagnetization of natural remanent
161 magnetization (NRM) was conducted using the 2-G Enterprises Model 760-R
162 cryogenic magnetometer (2G760) installed in a magnetically shielded (<300 nT)
163 space. AF demagnetization steps of 5-10 mT were used up to a maximum AF of 100
164 mT.

165 For bulk sediment mineralogy ~5-g samples were dried, pulverized, passed
166 through a 200 mesh sieve, and loaded into aluminum holders. Samples were X-rayed
167 from 5 to 65° 2θ with Cu K-alpha radiation (40 kV, 100 mA) using a step size of
168 0.02° 2θ and a counting time of 2 s per step on a D/max-2500 diffractometer (XRD)
169 equipped with a graphite monochromator with 1° slits in the laboratory of the First
170 Institute of Oceanography, SOA, China. Prior to the analysis, instrument was blank
171 corrected and all samples were measured under the same conditions. Peak areas were
172 estimated from XRD traces using Jade6.0 software, and semi-quantitative estimates of
173 bulk mineral percentages were calculated following Cook (1975). The windows (2θ),
174 range of spacings (A) and intensity factors of minerals were determined based on
175 Cook (1975) are listed in Table 1.

Samples for clay minerals determination (~5g) were first treated with H_2O_2 (10%) and HCl (1mol /L) to oxidize the organic matter and remove ~~the~~ carbonates, respectively. Clay fractions (< 2 μm) were obtained by the Atterberg settling tubes method according to Stoke's Law. Each sample was transferred to two slides by wet smearing. Samples were then air-dried prior to XRD analysis. One sample slide was air dried at 60 °C for 2 h and analyzed. The second sample was solvated with ethylene glycol in an underpressured desiccator for at least 24 h at 60 °C. Every ethylene-glycol solvated sample was measured twice: the first scanning was done from 3° to 30° 2θ with a step size of 0.02°, and the second scanning from 24° to 26° 2θ with a 0.01° step. The latter was run as a slow scan to distinguish the 3.54/3.58 Å kaolinite/chlorite double peak. Clay minerals were also identified by X-ray diffraction (XRD) using a D/max-2500 diffractometer with CuKα radiation (40 kV and 100 mA) in the laboratory of the First Institute of Oceanography, SOA, China. Peak areas representing the clay mineral groups were estimated from glycolated XRD traces using the17 Å smectite, 10 Å illite, and 7 Å chlorite plus kaolinite peaks. Chlorite (004) was identified at 3.54Å and kaolinite (002) at 3.58Å (Biscaye, 1964), respectively. Semi-quantitative estimates of clay mineral percentages were calculated by means of Biscaye's factors (1965).

To enhance the interpretation of downcore proxy distributions, Principal Component Analysis (PCA) was performed in MATLAB [MathWorks, 2014]. PCA included all analyzed mineralogical proxies along with main grain-size groups (clay, silt, fine to medium sand (63-250μm), and coarser grains), Ca and Mn concentrations

198 (ICP-OES), and foraminiferal numbers.

199

200 # 4. Results

201 ## 4.1 General stratigraphy

202 As common for sediment cores from the Arctic Ocean (e.g., Jakobsson et al.,
203 2000; Polyak et al., 2004, 2009; Spielhagen et al., 2004; Stein et al., 2010a, b), core
204 ARC4-BN05 displays distinct cycles in sediment color and composition expressed in
205 interlamination of dark brownish and lighter-colored grayish muds (silty clays, clay
206 silts and sandy silt), with coarser dropstones occurring in several layers. This color
207 cyclicity is approximated by changes in sediment lightness that largely mirrors the
208 content of Mn (Fig. 3), consistent with other studies from the Arctic Ocean (e.g.,
209 Jakobsson et al., 2000; Polyak et al., 2004; Adler et al., 2009). We identify 18
210 distinctly brown units, from B1 to B18, characterized by elevated content of Mn (Fig.
211 3). Another prominent lithostratigraphic feature in the western Arctic Ocean, widely
212 used for core correlation, is pink-white to whitish layers (PW) rich in detrital
213 carbonates (e.g., Clark et al., 1980; Polyak et al., 2009; Stein et al., 2010a, b). We
214 identify three major PW layers expressed both visually and in high Ca content (Fig.
215 3).

216 Foraminiferal abundances are generally high (mostly >50% of >63μm grains) in
217 brown units, except for B11-B13 and below B17-B18, and are very low to absent in
218 grey units. This pattern is consistent with foraminiferal stratigraphy reported in earlier

219 studies from the western Arctic Ocean (e.g., cores NP-26, HLY0503-JPC6 & 8,
220 P1-92AR-P23 & 39: Polyak et al., 2004, 2013; Adler et al., 2009; Cronin et al., 2013;
221 Lazar and Polyak, 2016).
222
223 **4.2 AMS ^{14}C dating**
224 The measured AMS ^{14}C ages of core ARC4-BN05 were calibrated to calendar
225 ages based on calibration using CALIB 7.10 (http://calib.org/calib/calib.html) (Table
226 2). The reservoir corrections of 790 and 1400 years were applied to Holocene and
227 glacial-age samples, respectively, according to Coulthard et al. (2010) and Hanslik et
228 al. (2010). Same corrections have also been applied to ^{14}C ages in core 03M03 from
229 the Chukchi Abyssal Plain (Fig. 2; Wang et al., 2013).
230
231 **4.3 Paleomagnetic stratigraphy**
232 While detailed paleomagnetic investigation is not an objective of this paper, we
233 utilize the inclination data for an independent stratigraphic constraint in line with
234 earlier studies (e.g., Jakobsson et al., 2000; Spielhagen et al., 2004; Polyak et al.,
235 2009). Paleomagnetic inclination in core ARC4-BN05 shows mostly positive values
236 oscillating around +70° in the upper part of the core, with a major polarity change
237 occurring at ~120 cm (Fig.3). A similar inclination drop has been identified in
238 multiple sediment cores across the Arctic Ocean in the same stratigraphic position
239 within estimated MIS 7, although the nature of this change in paleomagnetic

240 characteristics is not well understood (e.g., Jakobsson et al., 2000; Polyak et al., 2009;
241 Xuan and Channell, 2010).

242 Other paleomagnetic parameters, such as magnetic susceptibility (MS), can
243 provide additional correlation means (e.g., Sellén et al., 2010). Two prominent peaks
244 in MS occur in the intervals between units B7/B8 and B10/ B11 (Fig. 3).

245

246 **4.4 Grain size and dropstones**

247 Based on the results of grain-size analysis, sediment in core BN05 can be
248 generally classified as sandy mud, poorly to very poorly sorted, mostly coarse-skewed,
249 and strongly leptokurtic (peaked). Generally, silt and clay predominate grain-size
250 composition (33-60% and 23-61%, respectively), but coarser particles also make a
251 considerable contribution, with up to >30% peak contents of sand (>63μm) (Fig. 4a).
252 Coarse size fractions, from coarse silt to various sand fractions (e.g., >63, >125,
253 and >250 μm) mostly co-vary downcore.

254 Grain size distribution is mostly polymodal with three distinct major modes
255 centered at ~4, 7-7.5, and 85-90 μm, plus a smaller but consistent mode at ~400-450
256 μm (Fig. 4b), which can be approximated by clay (<4 μm), silt, and sand size
257 fractions. Mode 1 (4-μm) is overall most common in core BN05, occurring mostly in
258 combination with the fine- and/or coarse-sand mode, but also forming very
259 fine-grained intervals (e.g., at 37 cm, Fig. 4b). Mode 2 (7-7.5 μm) is common in the
260 lower part of the core (below ~175 cm), where it mostly co-occurs with mode 1 and

coarse-grain tail, and also in distinct grey units around 30-40 and 90-100 cm in combination with the fine-sand mode 3 (e.g., 39 and 93 cm, Fig. 4b).

Several core intervals contain large rock fragments >5 mm (dropstones). These rock fragments are mostly poorly rounded, subangular to angular in shape. Composition of sampled dropstones is illustrated in Fig. 4c. Most dropstones are represented by dolomite and low metamorphic quartz sandstone fragments of up to 5 cm in diameter. Also found were individual dropstones composed of volcanic rock and shale, as well as a few greisen dropstones near the base of the core.

4.5 Sediment mineralogy

The clay assemblage in samples from core ARC4-BN05 mainly consists of illite, chlorite, kaolinite and smectite (Fig. 5). The illite group is overall the major constituent of the clay mineral fraction, ranging between 43% and 73%. Its downcore distribution pattern is opposite to that of the three other major clay-mineral groups - kaolinite, chlorite, and smectite, which mostly co-vary except for some lithostratigraphic intervals, such as PW layers. Elevated content of these clay minerals is characteristic for grayish sedimentary units.

The bulk mineral assemblage in core ARC4-BN05 mainly consists of quartz, K-feldspar, plagioclase, calcite, dolomite and pyroxene (Fig. 5). Quartz is generally the most abundant mineral ranging between 20% and 51% and typically peaking in grayish sediment units. K-feldspar, plagioclase and pyroxene (mainly augitic) mostly

co-vary, with peaks in grey units in the upper part of the core, but more in brown units in the lower part starting from unit B10. Calcite has a high content in brown units of the upper part and much lower values below unit B9. Dolomite distribution shows distinct peaks reaching up to 53%, with the highest peaks occurring in the PW layers. Similar to other minerals, the pattern of dolomite distribution changes around unit B10, with maxima in thick grey units below and in thin interlayers within brown units above this stratigraphic level.

4.6 Principal Component Analysis

The first three Principal Components identified by PCA with a Varimax rotation account for 19%, 18%, and 17% of the total variance. This relatively low and evenly distributed communality of the leading PCs reflects a complexity of multi-proxy variables characterizing sedimentary environments and provenance, and their strong variability occurring over multiple climatic cycles. Despite this variability, the PCs identify several robust variable groups as shown in the PC loading score plots (Fig. 6). Most of the groupings are well reproduced in PC1-2 and PC2-3 plots, with just a few differences, such as a configuration of coarse grain-size fractions (high PC1 loading score for silt vs. high PC3 score for fine sand).

5. Discussion

5.1 Stratigraphic framework

As no single existing chronostratigraphic method can comprehensively constrain

304 the age of the Arctic Ocean Pleistocene sediments, the age model for core
305 ARC4-BN05 was developed by correlating multiple proxies (such as paleomagnetic,
306 foraminiferal, and lithological) to earlier established Arctic Ocean stratigraphies (e.g.,
307 Adler et al., 2009; Polyak et al., 2009, 2013; Stein et al., 2010a), combined with ^{14}C
308 ages in the youngest part of the record (~~e.g.,~~ Fig. 7).

309 The two ^{14}C dates from the uppermost, 10-cm-thick brown sedimentary unit (B1)
310 in core ARC4-BN05 clearly identify its Holocene age (Table 2; Fig. 3). Compilations
311 of ^{14}C ages from the surficial and downcore sediments in the western Arctic Ocean
312 (Polyak et al., 2009; Xiao et al., 2014) indicate that the age of this unit extends from
313 ~2-3 ka on top to ~10-11 ka at the bottom contact, although an accurate estimate is
314 impeded by the uncertainties with the reservoir ages.

315 Two ^{14}C dates of ca. 42-44 ka from the brown unit B2 (Table 2; Fig. 3)
316 apparently fall into MIS 3, consistent with earlier stratigraphic results (e.g., Polyak et
317 al., 2004, 2009; Adler et al., 2009; Stein et al., 2010a). These ages should be, however,
318 considered as crude estimates as they are close to the ^{14}C dating limit, and the age
319 distribution in B2 has common inversions (e.g., Polyak et al., 2009). In cores with
320 relatively elevated sedimentation rates this unit occurs as two distinct brown layers,
321 indicated in some papers as B2a and B2b (e.g., Stein et al., 2010a, b; Wang et al.,
322 2013). In core ARC4-BN05 this partitioning is less apparent due to low sedimentation
323 rates, but the brownish sediment on top of the coarse detrital carbonate peak PW/W3,
324 typically located between B2a and B2b, probably corresponds to B2a.

325 An abrupt increase in sediment age between closely spaced B1 and B2 in core

326 ARC4-BN05 suggests a very condensed section or a hiatus between MIS 1 and MIS 3.
327 This age distribution is common for the western Arctic Ocean, and has been attributed
328 to very low to no sedimentation due to a very solid sea-ice cover or an ice shelf during
329 the Last Glacial Maximum in MIS 2 (e.g. Polyak et al., 2009; Wang et al., 2013).
330 Below the range of ^{14}C ages the age model is based entirely on proxy
331 correlations with earlier developed Arctic Ocean stratigraphies (e.g., Fig. 7). This
332 correlation is enabled by the cyclic nature of sediment lithology and attendant proxies,
333 where brown and grayish units generally correspond to interglacial (or major
334 interstadial) and glacial climatic intervals, respectively (e.g., Jakobsson et al., 2000;
335 Polyak et al., 2004, 2009; Adler et al., 2009; Stein et al., 2010a, b). In addition,
336 correlation tie points are provided by rare or unique events, such as prominent detrital
337 carbonate peaks (PW/W), major paleomagnetic inclination swings, and changes in
338 foraminiferal assemblages and abundance pattern.
339 According to this approach, we identify foraminiferal- and Mn-rich brown units
340 B3-B7 and B8-B10 as warm substages of MIS 5 and 7, respectively (Figs. 3, 7). This
341 age assignment is corroborated by the prominent detrital carbonate peaks PW2 and 1
342 near the bottom of MIS 5 and 7, respectively. Furthermore, the principal drop in
343 paleomagnetic inclination in core ARC4-BN05 occurs in the lower part of MIS 7,
344 consistent with many cores from the Arctic Ocean (e.g., Jakobsson et al., 2000;
345 Spielhagen et al., 2004; Adler et al., 2009; Polyak et al., 2009). Solidly grayish,
346 foraminiferal and Mn-poor unit separating brown units B2 and B3 is accordingly
347 considered as related to glacial MIS 4, and a similar unit between B7 and B8 – to MIS

348 6. It is possible, however, that most of the fine-grained, greyish sediment was
349 deposited during deglaciations following the actual glacial intervals, which may have
350 been very compressed, similar to the LGM.

351 Stratigraphy below MIS 7 has been less investigated in prior studies, and
352 therefore the age model for the lower part of the core is more tentative. Nevertheless,
353 a prominent oldest foraminiferal peak in units B14-B16 (Fig. 3) allows us to identify
354 these units as MIS 11 by comparison with other microfaunal records reported from
355 the western Arctic Ocean (e.g., Cronin et al., 2013; Polyak et al., 2013). MIS 13 and
356 15 have been tentatively assigned to Units B17 and B18 underlying a prominent grey
357 interval attributed to MIS 12. Overall, the record in core ARC4-BN05 is estimated to
358 represent the last ca. 0.5-0.6 Ma, that is, most of the middle to late Quaternary with an
359 average sedimentation rates of 4-5 mm/ka.
360

361 **5.2 Depositional environments and sediment provenance**

362 Distribution of various terrigenous components in Arctic sediment records
363 carries information on sediment sources and depositional environments, and thus
364 paleocirculation and changes in paleoclimatic conditions, such as connection to other
365 oceans and build-up/disintegration of ice sheets (e.g., Bischof and Darby, 1997;
366 Krylov et al., 2008; Polyak et al., 2009; Stein et al., 2010a, b; Yurco et al., 2010;
367 Fagel et al., 2014). We utilize the data on clay and bulk minerals along with the grain
368 size and total Ca and Mn distribution in core ARC4-BN05 to reconstruct changes in

369 glacial conditions and circulation in the western Arctic Ocean during several glacial
370 cycles extending to estimated ca. 0.5-0.6 Ma. In this work we capitalize on earlier
371 studies on the distribution of bulk and/or clay minerals in surface and downcore
372 Arctic Ocean sediments (e.g., Vogt, 1997; Stein, 2008; Krylov et al., 2014; Zou,
373 2016), corroborated by more targeted provenance proxies, such as radiogenic isotopes
374 (Bazhenova, 2012; Fagel et al., 2014), heavy minerals (Stein, 2008; Kaparulina et al.,
375 2015), composition of coarse debris (Bischof et al., 1996; Wang et al., 2013), and
376 iron-oxide grains (e.g., Bischof and Darby, 1997; Darby et al., 2002).
377

378 **5.2.1 Grain size and depositional processes**

379 A variable, mostly multimodal distribution of grain size in core BN05 indicates
380 multiple controls on sediment delivery and/or deposition. The prevailing mode 1 at ~4
381 μm, often in variable combinations with the fine-sand mode, is common for brown
382 units, except for the oldest layers (estimated MIS 13/15 and partly 11). This pattern is
383 similar to grain-size distribution with an average mode at ~3.4 μm reported for
384 Holocene sediments across the Arctic Ocean (Darby et al., 2009). Furthermore,
385 sediment in core BN05 with the same mode also makes up the most fine-grained
386 intervals in glacial/deglacial units, such as MIS 4 and 6 (Fig. 4b). We infer that mode
387 1 represents some combination of deposition from sea ice and from suspension that
388 could result from winnowing of fines from the basin margins and ridges during
389 interglacials, as well as overflow plumes discharged by retreating glaciers during

390 glacial/deglacial intervals. An occurrence of apparently similar grain-size pattern in
391 interglacial and fine-grained glacial/deglacial intervals might indicate a convergence
392 of glacial erosion processes with those related to sea-ice formation and transportation.
393 A similar grain-size interpretation has been earlier proposed for sediment from the
394 Canada Basin with the principal mode at ~2 μm (Clark et al., 1980). This apparent
395 discrepancy may be related to the methodological offset between grain size
396 determined by the pipette method vs. laser diffraction, where the latter produces larger
397 diameters for fine sediment, especially in the presence of platy particles (Beuselinck
398 et al., 1998; Ramaswamy and Rao, 2006).

399 Mode 2 centered at 7-7.5 μm is more stratigraphically restricted. Its combination
400 with the fine-sand mode (e.g., Fig. 4b) is characteristic for coarser grained portions of
401 MIS 4, 6, and 12, which also have a specific mineralogical composition (PC loading
402 group 4: Fig. 6; Table 3). This distinct stratigraphic pattern suggests that the
403 formation of this sediment was related to glacial/deglacial processes; however, the
404 prevailing grain size mode arount 7-7.5 μm is too coarse for suspension plumes and
405 too fine for massive deposition from icebergs. On the other hand, fine to medium silts,
406 susceptible to intermediate currents, are common for turbiditic deposits, including
407 glacigenic environments (e.g., Wang and Hesse, 1996; Hesse and Khodabaksh, 2016).
408 We propose that mode 2 sediment type is related to glacial underflows that formed
409 debris lobes on glaciated margins grading into turbidites in the adjacent basins, along
410 with iceberg-rafted debris. Multiple debris lobes have been mapped on the Chukchi
411 and East-Siberian slopes in association with glacigenic diamictons on the margin

412 (Jakobsson et al., 2008; Niessen et al., 2013; Dove et al., 2014). Close to the margins
413 glacioturbidites can form deposits of several meters thick (Polyak et al., 2007), but
414 thin out towards the inner parts of the basins, such as the BN05 site. In particular,
415 deposits similar to fine-grained turbidites, attributed to MIS 4/lower MIS 3, have been
416 recovered from the Northwind and Chukchi basins affected by glacigenic inputs from
417 the Chukchi and East Siberian margins, respectively (Polyak et al., 2007; Matthiessen
418 et al., 2010; Wang et al., 2013). In the Chukchi Basin this unit, correlative to a much
419 thinner MIS 4 interval in core BN05, is characterized by a high content of fine silt
420 with a peaky downcore distribution (Wang et al., 2010, 2013).
421 Additionally, modes 1 and 2 make up a bimodal distribution in the lowermost
422 part of the core – mostly in estimated MIS 13/15 and near the bottom of MIS 11. The
423 predominant stratigraphic position in brown units makes unlikely the glacigenic origin
424 of this sediment. We hypothesize that this grain-size pattern reflects a combination of
425 "normal" interglacial environments with winnowed silts deposited by downwelling of
426 shelf waters enriched in dense brines. Although no observational evidence exists for
427 such waters penetrating deeper than the halocline (~200 m) under modern Arctic
428 conditions, periods of stronger cascading in the past have been inferred from sediment
429 distribution on the slopes (Darby et al., 2009) and some sedimentary proxies, such as
430 radiogenic isotopes (Haley and Polyak, 2013; Jang et al., 2013). The bimodal
431 distribution of fine sediment in the lower part of the record is accompanied in most
432 samples by a small but consistent coarse-sand mode (400-450 μm), likely indicating
433 the presence of iceberg rafting.

Coarse sediment, up to dropstones of several cm large, is a consistent feature in core BN05. In the apparent absence of strong current control on sedimentation, except for some shelf areas, and a pervasive presence of floating ice, coarse sediment in the Arctic Ocean is typically attributed to ice rafting, including sea ice and icebergs (e.g., Stein, 2008; Polyak et al., 2010, and references therein). Sedimentological studies in areas of sea-ice formation or melting and in ice itself indicate that sediment carried by sea ice in the Arctic Ocean is predominated by silt and clay, while coarser fractions are of minor importance (Clark and Hanson, 1983; Nürnberg et al., 1994; Hebbeln, 2000; Darby, 2003; Dethleff, 2005; Darby et al., 2009). Some studies suggest a higher content of sand in ice formed at the sea floor (anchor ice) (Darby et al., 2011), but the contribution of this source yet needs to be evaluated. Furthermore, the role of sea ice on sedimentation in the Arctic Ocean is not clear for glacial intervals, when most of the sediment entrainment areas were exposed or covered by ice sheets. In contrast, in iceberg-rafted sediment, deposited mostly in glacial/deglacial environments, the content of large size fractions, from sand to boulders, is typically high, in excess of 10-20% (Clark and Hanson, 1983; Dowdeswell et al., 1994; Andrews, 2000). Thus, elevated content of coarse sediment can be regarded as a good indicator of intense iceberg rafting. Such events are not probable during full interglacials, exemplified by modern conditions, but most likely occurred at times of instability and disintegration of ice sheets that extended to the Arctic Ocean in the past (e.g., Spielhagen et al., 2004; Stokes et al., 2005; Polyak et al., 2009).

In core BN05, coarse fractions (from coarse silt to sand) measured at different

sizes show very similar distribution patterns (Fig. 4a), indicating the same predominant delivery mechanism, that is, iceberg rafting. This pattern is reflected in a good correlation of fine to medium sand (63-250 μm) with coarser, >250μm fractions, that defines one of the PC loading groups (Fig. 6, Table 3). Increased coarse-grain content mostly characterizes grayish units, especially near gray-to-brown sediment transitions, and the PW layers, but also occurs in brown units in the upper part of the record. The latter peaks enriched in detrital carbonates (high dolomite and total Ca) represent interstadial or incomplete interglacial conditions, such as MIS 3, MIS 5a, and parts of MIS 7.

A common occurrence (separate or combined) of two coarse grain modes, around 85-90 and 400-450 μm, may indicate different sources for iceberg-rafted material or different thresholds for glacial disintegration of various rock types. While a more thorough interpretation requires further research, we note that grain-size mode 1 may co-occur with both fine-and coarse-sand modes, mode 2 – only with the fine-sand mode, and bimodal 1/2 sediment type – only with the coarse-sand one.

5.2.2 North American provenance

One of the most robust PC loading groups is distinctly characterized by high loadings of dolomite, total Ca content, and quartz/feldspar index (Group 2: Fig. 6, Table 3). Dolomite is known as a robust indicator of the North American provenance in the western Arctic, especially in relation to glacial inputs (e.g., Vogt, 1997; Zou,

2016). Dolomite is the main contributor of total Ca in sediment cores from the western Arctic Ocean, with an especially high content in multiple coarse-grain peaks (Bischof et al., 1996; Phillips and Grantz, 2001; Polyak et al., 2009; Stein et al., 2010a, b). This dolomite is related to the extensive, carbonate-rich Paleozoic terrane in the northern Canada (North American Platform; Fig. 1) that has been repeatedly eroded during the Pleistocene by the LIS. The distribution of dolomite in Arctic sediment cores can thus be used for reconstructing the history of the LIS sedimentary inputs.

Consistent with dolomite distribution in many other cores from the western Arctic Ocean, ~~its~~ overall high content in core ARC4-BN05 has major peaks corresponding to visually identifiable PW/W layers enriched in coarse debris (Fig. 5). As has been suggested in earlier studies (e.g., Stokes et al., 2005; Polyak et al., 2009), we infer that the dolomite peaks are related to pulses of massive iceberg discharge from the LIS during the periods of its destabilization and disintegration. Furthermore, radiogenic isotope studies demonstrate that fine sediment in the dolomitic peaks also has North American provenance (Bazhenova, 2012; Fagel et al., 2014). These results indicate that dolomite may have been transported not only by icebergs, but also in meltwater plumes coming during deglaciations from the Canadian Archipelago or the Mackenzie River.

As noted above, a change in the stratigraphic pattern of dolomite distribution occurs around unit B10 estimated to correspond to the lower part of MIS 7 (Fig. 5). In older sediments dolomite maxima co-occur with glacial (predominantly gray) intervals, whereas, in the younger stratigraphy dolomite peaks in brown sediment or

499 grayish interlayers within brown units (MIS 3, 5, and 7), presumably corresponding to
500 transitional paleoclimatic environments, such as interstadials or stadials within
501 complex interglacial stages.

502 Another mineral indicator related to the North American provenance is a
503 quartz/feldspar ratio due to a considerable presence of sedimentary rocks enriched in
504 quartz, but not feldspar, in the Canadian Arctic in comparison with the Siberian
505 margin (e.g., Vogt, 1997; Zou, 2016; Kobayashi et al., 2016). In core ARC4-BN05
506 the distribution of this index is generally similar to dolomite, except for some peak
507 intervals, notably low Qz/Fsp values in PW1 and 3 (Fig. 6).
508

509 **5.2.3 Siberian provenance**

510 Mineral proxies potentially linked to Siberian provenance make two distinct
511 groups, as reflected in the PCA results (Groups 3 and 4: Fig. 6, Table 3). Group 3
512 comprises primarily pyroxene, feldspar, and plagioclase, and strongly anticorrelates
513 with the North-American proxies, such as Qz/Fsp and dolomite. The downcore
514 distribution pattern of this group changes from the affinity to interglacials in the lower
515 part of the record to peaks in glacial/deglacial intervals related to MIS 4 and 6. The
516 major source for pyroxene in the Arctic Ocean is the Siberian trap basaltic province
517 that drains to the Kara Sea and western Laptev Sea (Fig. 1; Washner et al., 1999;
518 Schoster et al., 2000; Krylov et al., 2008). On the other hand, basaltic rocks related to
519 the Okhotsk-Chukotka province (Fig. 1) may have also provided a significant source of

pyroxenes, as exemplified in surface sediments by a relative pyroxene enrichment in the Chukchi Basin on the background of overall low values in the western Arctic Ocean (Dong et al., 2014). Distributions of feldspar and plagioclase at the Siberian margin show elevated contents occurring both in the western Laptev Sea and the East Siberian Sea (Zou, 2016).

Based on a considerable affinity of the pyroxene-feldspar group to brown units and a lack of correlation with coarse sediment fractions, we infer that it is primarily related to sea-ice transport during interglacial/deglacial intervals, with sources potentially including the East Siberian margin and more westerly areas. The difference in both the sources and delivery processes from the LIS proxies may explain an especially strong opposition of these groups. Multiple studies suggest that sea ice from the Kara and Laptev seas may transport sediments to the Canada Basin under favorable atmospheric conditions, such as the positive phase of the Arctic Oscillation (Behrends, 1999; Darby et al., 2003; Darby et al., 2004; Yurco et al., 2010; Darby et al., 2012), although it remains to be investigated, to what extent this circulation pattern could have provided a significant sediment source for the western Arctic Ocean in the Pleistocene.

5.2.4 East-Siberian Ice Sheet

The other group with a potentially Siberian provenance (Group 4: Fig. 6, Table 3) comprises clay minerals smectite, kaolinite, and chlorite, and is related to overall

541 coarse sediment, especially consistently to fine sand (63-250 μm). This composition is
542 especially characteristic for intervals estimated as MIS 4, 6, and 12. The association
543 of clay minerals with coarse sediment is unusual and suggests that they may have
544 been derived by glacial erosion of source hard rocks. This linkage has been elaborated
545 for kaolinite distribution in the Barents Sea and central Arctic Ocean (Junttila, 2007;
546 Vogt and Knies, 2009; Krylov et al., 2014). While kaolinite sources, such as
547 Meso-Cenozoic paleosols and shales, are mostly known in the western Arctic from
548 northern Alaska and Canada (Naidu et al., 1971; Darby, 1975; Dalrymple and Maass,
549 1987), kaolinite weathering crusts have been also described from the East Siberian
550 margin (Slobodin et al, 1990; Kim and Slobodin, 1991). Smectite, which is typically
551 related to chemical weathering of basic rocks has been mostly associated in Arctic
552 sediments with delivery from Siberian trap basalts (Fig. 1) as reflected in the surface
553 sediments, suspended particulate material, and sea-ice samples from the Kara Sea and
554 western Laptev Sea (Stein et al., 1994; Wahsner et al., 1999; Schoster et al., 2000;
555 Dethleff et al., 2000). Peaks of smectite related to that source are especially
556 charcteristic for deglacial intervals in sediment cores from the eastern Arctic Ocean
557 (Vogt and Knies, 2008). However, considerable sources of smectite also exist further
558 east along the Siberian margin due to basaltic outcrops related to the
559 Okhotsk-Chukotka volcanic province (Fig. 1), resulting in high content of smectite in
560 surface sediments of the East Siberian and Chukchi seas (Naidu et al., 1982;
561 Viscosi-Shirley et al., 2003; Nwaodua et al., 2014). Chlorite is also common in
562 surface sediments and suspended particulate material at the East Siberian margin

563 (Dethleff et al., 2000; Viscosi-Shirley et al., 2003). Modern and Holocene sediments
564 on the Chukchi shelf are especially enriched in chlorite due to advection from the
565 North Pacific at high sea-level stands (Kalinenko, 2001; Ortiz et al., 2009; Nwaodua
566 et al., 2014; Kobayashi et al., 2016), however this mechanism is only applicable to
567 interglacial periods.

568 We infer that sediment with a concerted enrichment in smectite, kaolinite, and
569 chlorite clay minerals associated with coarse fractions was transported to the Canada
570 Basin primarily in relation to the existence of large ice sheets in northern East Siberia
571 during glacial periods. Radiogenic isotope signature in upper Quaternary records from
572 the Mendeleev Ridge also indicates that the Okhotsk-Chukotka volcanic rocks
573 provided one of the principal end members, especially during MIS 4 and 6
574 (Bazhenova, 2012; Fagel et al., 2014). This sediment had to be transported into the
575 Arctic Ocean directly from the East-Siberian/Chukchi margin as the alternative
576 pathway via the Bering Sea only operated at high interglacial sea levels, when the
577 Bering Strait was open for throughflow (e.g., Keigwin et al., 2006; Ortiz et al., 2009).
578 Considering an affinity of the kaolinite-smectite-chlorite group with sediments
579 coarser than clays, corresponding to grain-size modes 2 and 3, their distribution across
580 the basin was likely related to iceberg rafting and glacial underflows, as discussed
581 above in section 5.2.1. A relatively fast and direct delivery mechanism by debris
582 flows and ensuing turbidites may explain a good preservation of fragile clay minerals,
583 normally not resistant to physical erosion.

584 Some early paleoglaciological studies proposed the existence of a thick

585 Pleistocene ice sheet centered over the East Siberian shelf (Hughes et al., 1977;
586 Grosswald and Hughes, 2002). The inference of former ice sheets/shelves in this
587 region is now corroborated by multibeam bathymetry and sub-bottom data revealing
588 multiple glacigenic features on the top and slopes of the Chukchi and East Siberian
589 margin (Polyak et al., 2001, 2007; Jakobsson et al., 2008, 2014, 2016; Niessen et al.,
590 2013; Dove et al., 2014). ESIS has also been reproduced by numerical paleoclimatic
591 modeling for a large Pleistocene glaciation exemplified by MIS 6 (Colleoni et al.,
592 2016). Sedimentary proxies indicative of the Okhotsk-Chukotka provenance in cores
593 from the Canada Basin provide an additional tool for reconstructing the ESIS history.
594

595 **5.2.5 Interglacial signature**

596 Data points from brown units make up a distinct PC loading group with Mn,
597 foraminiferal numbers, and fine sediment as lead variables (Group 1: Fig. 6; Table 3).
598 This composition is consistent with the modern-type Arctic Ocean environments
599 characterized by predominant controls of sediment deposition by sea ice, considerable
600 biological activity in summer, and high sea levels. The latter is important for
601 providing supply of Mn from the surrounding shelves (März et al., 2011; Löwemark
602 et al., 2014). The same condition may also control biological production, and thus
603 foraminiferal numbers, via export of nutrients from the marginal seas (e.g., Xiao et al.,
604 2014), although interaction of this factor with sea-ice conditions yet needs to be
605 clarified.

606 The two minerals having the closest distribution to PC loading group 1,
607 consistent with a predominant occurrence in brown, interglacial/major interstadial
608 units, are illite and calcite (Figs. 5, 6). Illite is a typical high-latitude clay mineral,
609 mainly supplied by physical weathering of metasedimentary and plutonic rocks
610 (Chamley, 1989; Junttila, 2007). High illite concentrations in surficial Arctic Ocean
611 sediments have been found in many areas including the Alaska margin and adjacent
612 Canada basin (Dong et al., 2014; Kobayashi et al., 2016), East Siberian Sea and the
613 adjacent part of the Laptev Sea (Wahsner et al., 1999; Kalinenko, 2001; Viscosi-
614 Shirley et al., 2003; Dethleff , 2005; Zou., 2016), and northern Greenland and
615 Svalbard regions (Stein et al., 1994). In core ARC4-BN05 illite has consistently high
616 values in generally fine-grained brown units (Fig. 5), although peak values may not
617 exactly coincide with those of Mn or foraminiferal numbers. In addition, illite shows a
618 prominent peak in a very fine-grained interval at ~35 cm within glacial/deglacial
619 sediment of estimated MIS 4. This distribution is consistent with the pattern in both
620 surface sediments and sediment cores, where illite is characteristic for fine-grained
621 sediment indicative of transportation by sea ice or in the water column (Krylov, 2014).
622 As shown by sediment-core studies, these mechanisms can provide high illite levels
623 under both interglacial (this study) and glacial/deglacial environments (Knies and
624 Vogt, 2003; Yurco et al., 2010). The latter is probably associated with deposition of
625 fine sediment from glacial overflows, as exemplified by the fine-grained part of MIS
626 4 deglaciation.
627 High contents of calcite in core ARC4-BN05 co-occur with high numbers of

foraminifers (Figs. 3 and 6), indicating that calcite in these sediments is to a large extent biogenic, consistent with earlier results from the study area (Stein et al., 2010a). Nevertheless, in the lower part of the record, where calcareous fossils are mostly not preserved, calcite shows a considerable affinity to dolomite, which corroborates a mixed, biogenic and detrital nature of calcite in Arctic Ocean sediments (e.g., Vogt, 1997).

5.3 Evolution of sedimentary environments

5.3.1 PC scores in the stratigraphic context

The stratigraphically changing pattern of sediment delivery and deposition, including cyclic glacial-interglacial fluctuations and longer-term changes, indicates complex interactions of climatic and oceanographic factors controlling depositional environments. To gain more insight into these changes, we plotted the distribution of PC scores grouped by individual glacial and interglacial stages, along with the PC loading interpretation (Fig. 8).

A long-term trend in interglacial environments is indicated by a shift from (1) predominantly Siberian to more North American provenance, especially strong in MIS 5 and 1, and (2) from negative to increasingly positive scores of interglacial proxies with a threshold around the bottom of MIS 7 (Fig. 8a). Glacial environments show an apparently more complex provenance change, with Siberian sources predominating early and late glacial stages (MIS 12-14 and MIS 4-6, respectively)

649 and Laurentide provenance controlling MIS 8 and 10 (Fig. 8b). In addition,
650 interglacial positive signature characterizes some intervals in MIS 4 and 6 as well as
651 intermittent (stadial) intra-MIS 3, 5, and 7 events. We note that MIS 2 is not
652 represented in this data due to its very compressed nature.
653

654 **5.3.1 Glacial environments**

655 The identified changes in sedimentary environments and provenance can be
656 explained by several types of controls, including configuration of ice sheets against
657 sea level and climatic conditions, sediment delivery mechanisms, and circulation. Ice
658 sheet sites and geometry at specific time intervals dictate the timing and location of
659 major sediment discharge events into the Arctic Ocean. Transportation mechanisms,
660 such as by icebergs, debris flows, or suspension plumes, further control sediment
661 delivery to specific sites. Finally, oceanic circulation affects the distribution of
662 sediment across the oceanic basins. This may include surface circulation driving sea
663 ice, icebergs, and surface plumes, deep circulation affecting turbidite/contourite
664 pathways, and downwelling of sediment-laden dense waters.
665 We infer that sedimentary variations observed in core BN05 and correlative
666 records from the western Arctic Ocean can be explained by the evolution of
667 surrounding ice sheets and associated changes in oceanic conditions, such as
668 circulation, sea ice, and biota. It has been known from early studies (e.g., Clark et al.,
669 1980; Winter et al., 1997) that glacial, notably LIS impact on the western Arctic

Ocean has been steadily increasing over the time span covered by sediment cores from this region. A recent investigation utilizing a more up-to-date stratigraphic paradigm estimated the timing of a step increase in LIS inputs as ca. 0.8 Ma (Polyak et al., 2013), consistent with the onset of major glaciations in the Northern Hemisphere (Head and Gibbard, 2015). Core BN05 provides a record of sediment deposition in the Canada Basin, and thus glacial inputs into the western Arctic Ocean during most of the time interval to follow.

Considering the overall gradual growth of Pleistocene Arctic ice sheets, we infer that the shift from Siberian to North American sources between MIS 12 and 10 was primarily related to the expansion of the LIS, especially the northwestern Keewatin sector that discharges into the western Arctic Ocean. However, its further growth may have had an opposite effect due to a more massive ice sheet that required warmer climatic conditions and/or higher sea levels to destabilize it. Based on data for the last glacial cycle, the Keewatin sector of the LIS rested mostly on relatively elevated terrane of the Canadian Archipelago and adjacent mainland, fringed by a narrow continental shelf and dissected by numerous channels providing conduits for ice streams and evacuation of icebergs at rising sea levels (Stokes et al., 2005, 2009; England et al., 2009; Margold et al., 2015). The latter events are illustrated in BN05 data by intra-MIS 5 stadials with a consistent LIS signature (Fig. 8b). Especially high LIS scores characterize PW layers 2 and 3 attributed to MIS 5d and late MIS 3, respectively. A similar, LIS-dominated pattern likely represents the last deglaciation as indicated by a number of provenance studies (e.g., Stokes et al., 2005; Bazhenova,

692 2012; Jang et al., 2013).

693 In comparison to the LIS, a presumably much smaller ESIS, formed on a broad
694 and overall flat East-Siberian/Chukchi margin (Niessen et al., 2013; Dove et al., 2014;
695 Colleoni et al., 2016), had to be responsive to sea-level changes even at low levels. It
696 may be possible that the ESIS also increased in size by MIS 6, known as a time of a
697 dramatic increase of glacial inputs from the Barents-Kara Ice Sheet into the eastern
698 Arctic Ocean (e.g., O'Regan et al., 2008). A synchronous MIS 6 expansion of both
699 North American and Siberian ice sheets and related ice shelves might explain the
700 deep-keel glacial erosion of the Lomonosov Ridge at modern water depths exceeding
701 1000 m (Jakobsson et al., 2016, and references therein).

702 A concurrent interpretation can be proposed with a focus on sediment
703 transportation processes as deposits of some glacial intervals, notably MIS 12 and
704 parts of MIS 4 and 6, are associated with grain size mode 2 potentially indicating
705 glacial debris flow/turbidite emplacement. Large debris flows entering the Chukchi
706 Basin and continuing as turbidites into Canada Basin, as exemplified by subbottom
707 sonar profiles (Niessen et al., 2013; Dove et al., 2014), may have overprinted
708 deposition from icebergs. We note that deposits of MIS 4 and 6 also contain intervals,
709 where Siberian provenance is combined with interglacial positive scores (Fig. 8b) due
710 to their fine-grained composition along with high illite content. These sediments
711 likely represent deposition from suspension plumes, potentially marking especially
712 strong deglacial meltwater discharge. A prominent fine grained, finely laminated
713 interval within MIS 4 deglaciation (possibly extending into MIS 3) has been reported

714 from multiple cores across the Chukchi Basin – Mendeleev Ridge area (Adler et al.,
715 2009; Matthiessen et al., 2010; Bazhenova, 2012; Wang et al., 2013).

716 Under modern conditions the BN05 site is mostly controlled by the Beaufort
717 Gyre current circulation system, although can also be affected by the Transpolar Drift
718 during strong shifts in the Arctic Oscillation (Rigor et al., 2002). This setting
719 porobably applies to the Holocene and comparable interglacial conditions (Darby and
720 Bischof, 2004). Some authors suggested that during glacial periods the surface
721 circulation that controls pathways of iceberg and sea-ice drift may have been
722 considerably different from the modern pattern, with both North American and
723 Siberian sources shortcutting the Arctic Ocean towards the Fram Strait (Bischof and
724 Darby, 1997; Stärz et al., 2012). These changes would have potentially affected the
725 study area, possibly making it more exposed to the Siberian provenance than under
726 present conditions. However, the existing reconstructions based on very limited
727 records with only crude stratigraphic controls, need to be elaborated by spatially and
728 stratigraphically more representative data constraining past circulation changes. In
729 particular, glacial maxima may be elusive, especially in the western Arctic Ocean, due
730 to extremely low sedimentation rates or a hiatus, as exemplified by the Last Glacial
731 Maximum (Polyak et al., 2009; Poirier et al., 2012).

732 An overall integration of potential controls on sediment deposition in the study
733 area during major identified types of glacial environments are illustrated in Fig. 9.
734 More studies are needed to discriminate between different controls, including proxy
735 records providing higher resolution for target intervals as well as modeling

736 experiments to test spatial and stratigraphic variability in such factors as iceberg and
737 meltwater discharge and their ensuing distribution pathways.
738

739 ### 5.3.2 Interglacial environments

740 The long-term trend in interglacial environments reflected in a shift from
741 negative to increasingly positive scores of interglacial proxies with a threshold around
742 the bottom of MIS 7 (Fig. 8a) can be partially explained by the absence of calcareous
743 foraminifers in the lower part of the record. However, even MIS 11 that has abundant
744 foraminifers is in the interglacial negative domain, suggesting more controls. One
745 possibility is that this trend was related to the evolution of circum-Arctic ice sheets
746 that would have inevitable incurred changes in oceanic conditions, such as circulation
747 and sea ice. An expansion of perennial sea ice in the western Arctic Ocean near the
748 MIS 7 bottom has been proposed based on foraminiferal assemblages (Polyak et al.,
749 2013; Lazar and Polyak, 2016). This step change has been tentatively attributed to the
750 LIS growth that may have affected sea-ice conditions via increased albedo and/or
751 higher meltwater inputs. This inference is consistent with a change from Siberian to
752 North American provenance during interglacials in BN05 (Fig. 8a). In addition to a
753 more lingering LIS during interstadials/interglacials, this shift in provenance could be
754 related to a strengthening of the Beaufort Gyre as more sea ice filled the western
755 Arctic Ocean.
756 More limited sea-ice cover in the older part of the middle Pleistocene could have

757 also enhanced the production of dense brines at the Siberian margin, resulting in a
758 deeper convection and cascading of shelf sediments to the deep basin. This scenario
759 would explain an unusual grain-size composition of sediments in the older
760 interglacials combining mode 2, indicative of winnowed silt, with a typical
761 interglacial fine-grained mode 1.
762

763 ## 6. Summary and conclusions

764 Sediment core ARC4–BN05 was collected from the Canada Basin in the vicinity
765 of the Chukchi Plateau and the Mendeleev Ridge, Arctic Ocean, on the fourth Chinese
766 National Arctic Research Expedition (CHINARE-Ⅳ). Based on correlation to earlier
767 proposed Arctic Ocean stratigraphies (e.g., Adler et al., 2009; Stein et al., 2010a;
768 Polyak et al., 2013) and AMS ^{14}C dating of the youngest sediments, the BN05 record
769 covers the late to middle Quaternary (MIS 1-15, ca. 0.5-0.6 Ma). The core was
770 investigated for multiple sedimentary proxies including clay and bulk mineralogy,
771 grain size, paleomagnetism, elemental content, and planktonic foraminiferal numbers
772 with an average estimated age resolution of 4-5 ka per sample. This study, facilitated
773 by Principal Component Analysis of major paleoceanographic variables, provides
774 important new information about sedimentary environments and provenance in the
775 western Arctic Ocean on glacial time scales. The results enhance our knowledge on
776 the history of Arctic glaciations and interglacial conditions.
777 Glacially derived sediment can be discriminated between the North American

778 and Siberian provenance by their mineralogical and textural signature. In particular,
779 peaks of dolomite debris, including large dropstones, track the Laurentide Ice Sheet
780 (LIS) discharge events, while the East Siberian Ice Sheet (ESIS) inputs are inferred
781 from combined peaks of smectite, kaolinite, and chlorite associated with coarse
782 sediment. Siberian provenance is also identified from high content of pyroxene,
783 feldspar, and plagioclase, unrelated to coarse sediment. This sedimentary signature is
784 interpreted to indicate sea-ice transport from the Siberian margin during
785 interglacial/deglacial intervals. Full interglacial environments are characterized by
786 overall fine grain size, high content of Mn (and resulting dark brown sediment color),
787 and elevated contents of calcite and chlorite. Foraminiferal tests are abundant in
788 interglacial units in the upper part of the record (MIS 1-7) and estimated MIS 11, but
789 have very low numbers in other interglacials older than MIS 7, apparently due to
790 dissolution.

791 In addition to glacial-interglacial cyclicity, the investigated record indicates
792 variable impacts of LIS vs. ESIS on sediment inputs at different glacial events, along
793 with a long-term change in middle to late Quaternary sedimentary environments.
794 Based on the age model employed, major LIS inputs to the study area occurred during
795 MIS 3, intra-MIS 5 and 7 events, MIS 8, and MIS 10, while ESIS signature is
796 characteristic for MIS 4, MIS 6 and MIS 12. These differences may be related to
797 ice-sheet configurations at different sea levels, sediment delivery mechanisms
798 (iceberg rafting, suspension plumes, and debris flows), and surface circulation. A
799 long-term shift in the pattern of sediment inputs shows an apparent step change near

the estimated MIS 7/8 boundary (ca. 0.25 Ma), consistent with more sea-ice growth in the Arctic Ocean inferred from benthic foraminiferal assemblages (Lazar and Polyak, 2016). This development of Arctic Ocean paleoenvironments possibly indicates an overall glacial expansion at the western Arctic margins, especially in North America. Such expansion may have affected not only glacial, but also interglacial conditions via increased albedo and/or higher meltwater inputs, as well as a strengthening of the Beaufort Gyre circulation as more sea ice filled the western Arctic Ocean.

Acknowledgements

We are grateful to the term of the Chinese fourth Arctic scientific expedition for their assistance with sample collection. Special thanks are extended to Dr. Shijuan Yan for the help with sampling and to Dr. Quanshu Yan for the help in editing of the paper. This work was jointly supported by the Research Foundation of the First Institute of Oceanography, State Oceanic Administration of China (No. 2013G07, 2014G30), the Chinese Special Project of Arctic Ocean Marine Geology Investigation (No. CHINARE 2016-03-02), and the National Natural Science Foundation of China (No. 41306205, 41676053, 40176136).

References

[1] Adler, R. E., Polyak, L., Ortiz, J. D., Kaufman, D. S., Channell, J. E.T., Xuan, C., Grottoli, A. G., Sellén, E., Crawford, K. A.: Sediment record from the western Arctic Ocean with an improved Late Quaternary age resolution: HOTRAX core HLY0503-8JPC, Mendeleev Ridge, **Global and Planetary Change**, 68,18-29,2009.

[2] Andrews, J. T.: Icebergs and iceberg rafted detritus (IRD) in the North Atlantic: Facts and assumptions, **Oceanography,** 13(3), 100–108, 2000.

[3] Basilyan, A.E., Nikol'skyi, P.A., Maksimov, F.E., Kuznetsov, V.Y.: Age of Cover Glaciation of the New Siberian Islands Based on 230Th/U-dating of Mollusk Shells, **Structure and Development of the Lithosphere,** Paulsen, Moscow, pp. 506-514, 2010.

[4] Bazhenova, E.: Reconstruction of late Quaternary sedimentary environments at the southern Mendeleev Ridge (Arctic Ocean), **PhD Thesis**, University of Bremen, Bremen, 83 p, 2012.

[5] Behrends, M.: Reconstruction of sea-ice drift and terrigenous sediment supply in the Late Quaternary: heavy-mineral associations in sediments of the Laptev-Sea continental margin and the central Arctic Ocean, **Reports on Polar Research,** 310, 1-167, 1999.

[6] Beuselinck, L., Govers, G., Poesen, J., Degraer, G., Froyen, L.:Grain-size analysis by laser diffractometry: comparison with the sieve-pipette method, **Catena,** 32, 193–208, 1998.

[7] Bischof, J. F. and Darby, D. A.: Mid-to Late Pleistocene ice drift in the Western Arctic Ocean: evidence for a different circulation in the past, **Science**, 277, 74–78, 1997.

[8] Bischof, J.F., Clark, D.L., Vincent, J.S.: Origin of ice-rafted debris: Pleistocene paleoceanography in the western Arctic Ocean, **Paleoceanography,** 11, 743–756, 1996.

[9] Biscaye, P.F.: Distinction between kaolinite and chlorite in recent sediments by X-ray diffraction, **American Mineralogist,** 49, 1281–1289, 1964.

[10] Biscaye, P.F.: Mineralogy and sedimentation of recent deep-sea clay in the Atlantic Ocean and adjacent seas and oceans, **The Geological Society America Bulletin,** 76, 803–832, 1965.

[11] Chamley, H.: Clay Sedimentology, **Springer**, Berlin. 623 pp, 1989.

[12] Clark, D. L., Whitman, R. R., Morgan, K. A., Mackey, S. D.: Stratigraphy and glacialmarine sediments of the Amerasian Basin, central Arctic Ocean, **Geological Society of America**, Special Paper, 181, 57, 1980.

[13] Clark, D. and Hanson, A.: Central Arctic Ocean sediment texture: a key to ice transport mechanisms. **In: Molnia, B.F. (Ed.), Glacial-Marine Sedimentation, Plenum Press**, New York, pp. 301–330, 1983.

[14] Clark, D. L., Chern, L. A., Hogler, J. A., Mennicke, C. M., Atkins, E. D.: Late Neogene climate evolution of the central Arctic Ocean, **Marine Geology,** 93, 69–94 ,1990.

[15] Colleoni, F., Kirchner, N., Niessen, F., Quiquet, A., Liakka, J.: An East Siberian ice shelf during the Late Pleistocene glaciations: Numerical reconstructions, **Quaternary Science Reviews,** xxx,1-16, 2016.

[16] Cook, H. E., Johnson, P.D., Matti, J.C., Zemmels, I.: Methods of sample preparation and X- ray diffraction data analysis, X-ray mineralogy laboratory, **In: Kaneps AG,** ed. Init Repts, DSDP XXVIII, 999 -1007, http: //www.deepseadrilling.Org/28/ volume/dsdp28- appendix-IV. Pdf, 1975.

[17] Coulthard, R.D., Furze, M.F.A., Pienkowski, A.J., Nixon, F.C., England, J.H.: New marine ΔR values for Arctic Canada, **Quaternary Geochronology,** 5, 419–434, 2010.

[18] Cronin, T.M., Polyak, L., Reed, D., Kandiano, E.S., Marzen, R.E., Council, E.A.: A 600-ka Arctic sea-ice record from Mendeleev Ridge based on ostracodes, **Quaternary Science Reviews,** 79, 157–167, 2013.

[19] Dalrymple, R.W. and Maass, O. C.: Clay mineralogy of late Cenozoic sediments in the CESAR cores, Alpha Ridge, central Arctic ocean, **Canadian Journal of Earth Science,** 24, 1562–1569, 1987.

[20] Darby, D.A.: Kaolinite and other clay minerals in Arctic Ocean sediments, **Journal of Sedimentary Petrology,** 45,272–279, 1975.

[21] Darby, D. A., Bischof, J. F., Jones, G. A.: Radiocarbon chronology of depositional regimes in the western Arctic Ocean, **Deep Sea Research Part II,** 44 (8), 1745–1757, 1997.

[22] Darby, D. A., Bischof, J. F., Spielhagen, R. F., Marshall, S. A., Herman, S. W.: Arctic ice export events and their potential impact on global climate during the Late Pleistocene, **Paleoceanography,** 17(2), 1025, doi:10.1029/2001PA000639, 2002.

[23] Darby, D. A.: Sources of sediment found in sea ice from the western Arctic Ocean, new insights into processes of entrainment and drift patterns, **Journal of Geophysical Research,** 108(C8), 3257, doi:10.1029/2002JC001350, 2003.

[24] Darby, D. A., and Bischof, J. F.: A Holocene record of changing Arctic Ocean ice drift, analogous to the effects of the Arctic Oscillation, **Paleoceanography,** 19, PA1027, doi:10.1029/2003PA000961, 2004.

[25] Darby, D.A., Polyak, L., Bauch, H.A.: Past glacial and interglacial conditions in the Arctic Ocean and marginal seas — a review, **Progress in Oceanography,** 71,129–144, 2006.

[26] Darby, D. A., Ortiz, J., Polyak, L., Lund, S., Jakobsson, M., Woodgate, R.A.: The role of currents and sea

ice in both slowly deposited central Arctic and rapidly deposited Chukchi-Alaskan margin sediments, **Global and Planetary Change,** 68, 58-72, 2009.

[27] Darby, D. A., Myers, W., Jakobsson, M., Rigor, I.: Modern dirty sea ice characteristics and sources: The role of anchor ice, **Journal of Geophysical Research**, 116: C09008, doi:10.1029/2010JC006675, 2011.

[28] Darby, D., Ortiz, J., Grosch, C., Lund, S.: 1,500-year cycle in the Arctic Oscillation identified in Holocene Arctic sea-ice drift. **Nature Geoscience** 5, 897–900, 2012.

[29] Dethleff, D. A., Rachold, V., Tintelnot, T., Antonow, M.: Sea-ice transport of riverine particles from the Laptev Sea to Fram Strait based on clay mineral studies, **International Journal of Earth Science,** 89, 496–502, 2000.

[30] Dethleff, D.: Entrainment and export of Laptev Sea ice sediments, Siberian Arctic, **Journal of Geophysical Research**—Oceans 110, C07009, doi:10.1029/2004JC002740, 2005.

[31] Dove, D., Polyak, L., Coakley, B.: Widespread, multi-source glacial erosion on the Chukchi margin, Arctic Ocean, **Quaternary Science Reviews,** 92, 112-122, 2014.

[32] Dong, L., Shi, X., Liu, Y., Fang,X., Chen, Z., Wang, C., Zou, J., Huang, Y.: Mineralogical study of surface sediments in the western Arctic Ocean and their implications for material sources, **Advances in Polar Science,** 25(3),192-203, 2014.

[33] Dowdeswell, J. A., Villinger, H., Whittington, R. J., Marienfeld, P.: Iceberg scouring in Scores by Sund and on the East Greenland continental shelf, **Marine Geology,** 111, 37–53 ,1993.

[34] Dyke, A. S., Andrews, J. T., Clark, P. U., England, J. H., Miller, G. H., Shaw, J., Veillette, J. J.: The Laurentide and Innuitian ice sheets during the Last Glacial Maximum, **Quaternary Science Review,** 21, 9–31, 2002.

[35] England, J.H., Furze, M.F.A., Doupé, J. P.: Revision of the NW Laurentide Ice Sheet: implications for paleoclimate, the northeast extremity of Beringia, and Arctic Ocean sedimentation, **Quaternary Science Review,** 28, 1573-1596, 2009.

[36] Fagel, N., Not, C., Gueibe, J., Mattielli, N., Bazhenova, E.: Late Quaternary evolution of sediment provenances in the Central Arctic Ocean: mineral assemblage, trace element composition and Nd and Pb isotope fingerprints of detrital fraction from the Northern Mendeleev Ridge, **Quaternary Science Reviews,** 92,140-154, 2014.

[37] Grosswald, M.G. and Hughes, T.J.: The Russian component of an Arctic Ice Sheet during the Last Glacial Maximum, **Quaternary Science Review,** 21, 121-146, 2002.

[38] Haley, B.A. and Polyak, L.: Pre-modern Arctic Ocean circulation from surface sediment neodymium isotopes, **Geophys. Res. Lett**., 40, 1–5, 2013.

[39] Hanslik, D., Jakobsson, M., Backman, J., Björck, S., Sellén, E., O'Regan, M., Fornaciari, E.,Skog, G.: Quaternary Arctic Ocean sea ice variations and radiocarbon reservoir age corrections, **Quaternary Science Reviews ,** 29, 3430–3441 , 2010.

[40] Head, M.J. and Gibbard, P. L.: Early-Middle Pleistocene transitions: linking terrestrial and marine realms, **Quaternary International,** 389, 7-46, 2015.

[41] Hebbeln, D.: Flux of ice-rafted detritus from sea ice in the Fram Strait, **Deep-Sea Research Part II,** 47, 1773–1790, 2000.

[42] Hesse, R. and Khodabakhsh, S.: Anatomy of Labrador Sea Heinrich layers, **Marine Geology,** 380, 44–66, 2016.

[43] Hughes, T.J., Denton, G.H., Grosswald, M.G.: Was there a late-Würm Arctic ice sheet? **Nature,** 266, 596-602, 1977.

[44] Jakobsson, M., Løvlie, R., Al-Hanbali, H., Arnold, E., Backman, J., Mörth, M.: Manganese and color cycle in Arctic Ocean sediments constrain Pleistocene chronology, **Geology,** 28, 23–26, 2000.

[45] Jakobsson, M., Polyak, L., Edwards, M., Kleman, J., Coakley, B.: Glacial geomorphology of the Central Arctic Ocean: the Chukchi Borderland and the Lomonosov Ridge, **Earth Surface Processes and Landforms,** 33, 526–545, 2008.

[46] Jakobsson, M., Andreassen, K., Bjarnadóttir, L. R., Dove, D., Dowdeswell, J. A., England, J.H., Funder, S., Hogan, K., Ingólfsson,Ó., Jennings, A., Larsen, N, K., Kirchner, N., Landvik, J.Y., Mayer, L., Mikkelsen, N., Möller, P., Niessen, F., Nilsson, J., O'Regan, M., Polyak, L., Nørgaard-Pedersen, N., Stein. R.: Arctic Ocean glacial history, **Quaternary Science Reviews,** 92, 40–67, 2014.

[47] Jakobsson, M., Nilsson, J., Anderson, L., Backman, J., Björk, G., Cronin, T.M., Kirchner, N., Koshurnikov, A., Mayer, L., Noormets ,R., O'Regan, M.,Stranne, C., Ananiev, R., Macho, N. B., Cherniykh, D., Coxall, H.,Eriksson, B., Flodén, T., Gemery, L., Gustafsson, O., Jerram, K., Johansson, C., Khortov ,A., Mohammad, R., Semiletov, I.: Evidence for an ice shelf covering the central Arctic Ocean during the penultimate glaciation, **Nature Communications ,** doi: 10.1038/ncomms10365, 2016.

[48] Jang, K., Han, Y., Huh, Y., Nam, S., Stein, R., Mackensen, A., Matthiessen, J.: Glacial freshwater discharge events recorded by authigenic neodymium isotopes in sediments from the Mendeleev Ridge, western Arctic Ocean, **Earth and Planetary Science Letters,** 369-370,148–157, 2013.

938 [49] Junttila, J.: Clay minerals in response to Mid-Pliocene glacial history and climate in the polar regions
939 (ODP, Site 1165, Prydz Bay, Antarctica and Site 911, Yermak Plateau, Arctic Ocean), **Acta Universitat**
940 **Ouluensis,** A 481,2007.
941 [50] Kalinenko, V.V.: Clay minerals in sediments of the Arctic Seas. **Lithology and Mineral Resources,** 36,
942 362–372, 2001.
943 [51] Kaparulina, E., Strand, K., Lunkka, J. P.: Provenance analysis of central Arctic Ocean sediments:
944 Implications for circum-Arctic ice sheet dynamics and ocean circulation during Late Pleistocene,
945 **Quaternary Science Reviews,** XXX, 1-11, 2015.
946 [52] Keigwin, L.D., Donnelly, J.P., Cook, M.S., Driscoll, N.W., Brigham-Grette, J.: Rapid sea-level rise and
947 Holocene climate in the Chukchi Sea, **Geology,** 34 (10), 861–864, doi:10.1130/G22712.1, 2006.
948 [53] Kim, B.I. and Slobodin, V.Ya.: Main stages of the evolution of East Arctic shelves of Russia and
949 Canadian Arctic in the Paleogene and Neogene, **In: Geologiya skladchatogo obramleniya**
950 **Ameraziiskogo subbasseina (Geology of the Folded Framing of the Amerasian Subbasin),** St.
951 Petersburg: Sevmorgeologiya, 104–116, 1991.
952 [54] Knies, J., Kleiber, H. P., Matthiessen, J., Müller, C., Nowaczyk, N.: Marine ice-rafted debris records
953 constrain maximum extent of Saalian and Weichselian ice-sheets along the northern Eurasian margin,
954 **Global and Planetary Change,** 31, 45–64, 2001.
955 [55] Knies, J. and Vogt, C.: Freshwater pulses in the eastern Arctic Ocean during Saalian and early
956 Weichselian ice-sheet collapse, **Quaternary Research,** 60, 243–251, 2003.
957 [56] Kobayashi, D., Yamamoto, M., TIrino, T., Nam, S.-I., Park, Y.-H., Harada, N., Nagashima, K., Chikita,
958 K., Saitoh, S.I.: Distribution of detrital minerals and sediment color in western Arctic Ocean and
959 northern Bering Sea sediments: changes in the provenance of western Arctic Ocean sediments since the
960 last glacial period, **Polar Science,** 10, 519–531, 2016.
961 [57] Krylov, A. A., Andreeva I. A., Vogt C., Backman J., Krupskaya V. V., Grikurov G. E., Moran K., Shoji H.:
962 A shift in heavy and clay mineral provenance indicates a middle Miocene onset of a perennial sea ice
963 cover in the Arctic Ocean, **Paleoceanography,** 23, PA1S06, doi:10.1029/2007PA001497, 2008.
964 [58] Krylov, A.A., Stein, R., Ermakova, L.A. Clay minerals as indicators of late quaternary sedimentation
965 constraints in the Mendeleev Rise, Amerasian Basin, Arctic Ocean, **Lithology and Mineral Resources,**
966 49, 103-116, 2014.
967 [59] Larsen, E., Kjær, K.H., Demidov, I.N., Funder, S., Grøsfjeld, K., Houmark-Nielsen, M.,Jensen, M.,

Linge, H., Lyså, A.: Late Pleistocene glacial and lake history of northwestern Russia, **Boreas,** 35, 394-424 , 2006.

[60] Lazar, K.B. and Polyak, L.: Pleistocene benthic foraminifers in the Arctic Ocean: Implications for seaice and circulation history, **Marine Micropaleontology,** 126, 19-30, 2016.

[61] Löwemark. L., März, C., O'Regan, M., Gyllencreutz, R. Arctic Ocean Mn-stratigraphy: genesis, synthesis and inter-basin correlation, **Quaternary Science Reviews,** 92, 97-111, 2014.

[62] Margold M., Stokes C. R., Clark C. D.: Ice streams in the Laurentide Ice Sheet: Identification, characteristics and comparison to modern ice sheets, **Earth-Science Reviews,** 143, 117–146, 2015.

[63] März, C., Stratmann, A., Matthiessen, J., Meinhardt, A., Eckert, S., Schnetger, B., Vogt, C., Stein, R., Brumsack, H.: Manganese-rich brown layers in Arctic Ocean sediments: composition, formation mechanisms, and diagenetic overprint. **Geochimica et Cosmochimica Acta,** 75, 7668–7687, 2011.

[64] Matthiessen, J., Niessen F., Stein, R., Naafs, B. D.: Pleistocene Glacial Marine Sedimentary Environments at the Eastern Mendeleev Ridge, Arctic Ocean, **Polarforschung,** 79 (2), 123 – 137, 2009 (erschienen 2010).

[65] Naidu, A.S., Burrell, D.C., Hood, D.W.: Clay mineral composition and geological significance of some Beaufort Sea sediments, **Journal of Sedimentary Petrology,** 41, 691–694, 1971.

[66] Naidu, A. S., Creager, J. S., Mowatt, T. C.: Clay mineral dispersal patterns in the north Bering and Chukchi Seas. **Marine Geology,** 47(1), 1-15, 1982.

[67] Niessen, F., Hong, J.K., Hegewald, A., Matthiessen, J., Stein, R., Kim, H., Kim, S., Jensen, L., Jokat, W., Nam, S.-I., Kang, S.-H.: Repeated Pleistocene glaciation of the East Siberian Continental Margin, **Nature Geoscience,** 6, 842-846, 2013.

[68] Nürnberg, D., Wollenburg, I., Dethleff, D., Eicken, H., Kassens, H., Letzig, T., Reimnitz, E., Thiede, J.: Sediments in Arctic sea ice: Implications for entrainment, transport and release, **Marine Geology,** 119, 185–214, 1994.

[69] Nwaodua, E.C., Ortiz J. D., Griffith E. M.: Diffuse spectral reflectance of surficial sediments indicates sedimentary environments on the shelves of the Bering Sea and western Arctic, **Marine Geology,** 355, 218–233, 2014.

[70] O'Regan, M., King, J., Backman, J., Jakobsson, M., Pälike, H., Moran, K., Heil, C., Sakamoto, T.,Cronin, T.M., Jordan, R.W.: Constraints on the Pleistocene chronology of sediments from the Lomonosov Ridge, **Paleoceanography,** 23, PA1S19, doi:10.1029/2007PA001551 , 2008.

[71] Ortiz, J.D., Polyak, L., Grebmeier, J.M., Darby, D., Eberl, D.D., Naidu, S., Nof, D.: Provenance of Holocene sediment on the Chukchi–Alaskan margin based on combined diffuse spectral reflectance and quantitative X-Ray diffraction analysis, **Global and Planetary Change,** 68 (no. 1–2), 73–84, 2009.

[72] Phillips, R. L. and Grantz, A.: Regional variations in provenance and abundance of ice-rafted clasts in Arctic Ocean sediments: Implications for the configuration of late Quaternary oceanic and atmospheric circulation in the Arctic, **Marine Geology,** 172, 91—115, 2001.

[73] Poirier, R.K., Cronin, T.M., Briggs Jr., W.M., Lockwood, R.: Central Arctic paleoceanography for the last 50 kyr based on ostracode faunal assemblages, **Marine Micropaleontology,** 88–89, 65–76, 2012.

[74] Polyak, L., Edwards, M.H., Coakley, B.J., Jakobsson, M.: Ice shelves in the Pleistocene Arctic Ocean inferred from glaciogenic deep-sea bedforms, **Nature,** 410, 453–459, 2001.

[75] Polyak, L. V., Curry, W. B., Darby, D. A., Bischof, J., Cronin, T. M.: Contrasting glacial/interglacial regimes in the Western Arctic Ocean as exemplied by a sedimentary record from the Mendeleev Ridge, **Palaeogeography, Palaeoclimatology, Palaeoecology,** 203, 73–93, 2004.

[76] Polyak, L., Darby, D.A., Bischof, J., Jakobsson, M.: Stratigraphic constraints on late Pleistocene glacial erosion and deglaciation of the Chukchi margin, Arctic Ocean, **Quaternary Research**, 67:234–245, doi:10.1016/j.yqres.2006.08.001, 2007.

[77] Polyak, L., Bischof, J., Ortiz, J.D., Darby, D.A., Channell, J.E.T., Xuan, C., Kaufman, D.S., Lovlie, R., Schneider, D.A., Eberl, D.D., Adler, R.E., Council, E.A.: Late Quaternary stratigraphy and sedimentation patterns in the western Arctic Ocean, **Global and Planetary Change,** 68, 5-17, 2009.

[78] Polyak, L., Alley, R.B., Andrews, J.T., Brigham-Grette, J., Cronin, T.M., Darby, D.A., Dyke, A.S., Fitzpatrick, J.J., Funder, S., Holland, M., Jennings, A.E., Miller, G.H., O'Regan, M., Savelle, J., Serreze, M., St. John, K., White, J.W.C., Wolff, E.: History of sea ice in the Arctic, **Quaternary Science Reviews,** 29, 1757-1778, 2010.

[79] Polyak, L., Best, K. M., Crawford, K. A., Council, E. A., St-Onge, G.: Quaternary history of sea ice in the western Arctic Ocean based on foraminifera, **Quaternary Science Reviews,** 79, 145-156, 2013.

[80] Ramaswamy V. and Rao P. S.: Grain Size Analysis of Sediments from the Northern Andaman Sea: Comparison of Laser Diffraction and Sieve-Pipette Techniques, **Journal of Coastal Research,** 22, 1000–1009, 2006.

[81] Rigor, I.G., Wallace, J.M., Colony, R.L.: Response of sea ice to the Arctic Oscillation, **Journal of Climate,** 15, 2648–2663, 2002.

[82] Rudels, B.: Arctic Ocean circulation. **Encyclopedia of Ocean Sciences, J.H. Steele, K.K. Turekian, S.A. Thorpe (Eds.-in-Chief)**, Elsevier, 211-225, 2009.

[83] Sharma, M., Basu, A.R., Nesterenko, G. V.: Temporal Sr-, Nd- and Pb isotopic variations in the Siberian flood basalts: implications for the plume-source characteristics, **Earth and Planetary Science Letters,** 113, 365-381, 1992.

[84] Slobodin, V.Ya., Kim, B.I., Stepanova, G.V., Kovalenko, F.Ya.: Differentiation of the Aion borehole section based on the biostratigraphic data, **In: Stratigrafiya i paleontologiya mezo-kainozoya Sovetskoi Arktiki (Stratigraphy and Paleontology of the Meso-Cenozoic in the Soviet Arctic)**, Leningrad: Sevmorgeologiya, 43–58, 1990.

[85] Spielhagen, R. F., Bonani, G., Eisenhauer, A., Frank, M., Frederichs, T., Kassens, H., Kubik, P. W., Mangini, A., Nörgaard-Pedersen, N., Nowaczyk, N. R., Schäper, S., Stein, R., Thiede, J., Tiedemann, R., Wahsner, M.: Arctic Ocean evidence for Late Quaternary initiation of northern Eurasian ice sheets, **Geology, 2**5, 783–786 ,1997.

[86] Spielhagen, R. F., Baumann, K. H., Erlenkeuser, H., Nowaczyk, N. R., Nørgaard-Pedersen, N.,Vogt, C., Weiel, D. Arctic Ocean deep-sea record of Northern Eurasian ice sheet history, **Quaternary Science Review,** 23, 1455–1483, 2004.

[87] Schoster, F., Behrends, M., Müller, C., Stein, R., Wahsner, M.: Modern river discharge in the Eurasian Arctic Ocean: Evidence from mineral assemblages and major and minor element distributions, **International Journal of Earth Science**, 89, 486–495, 2000.

[88] Sellén, E., O'Regan, M., Jakobsson, M.: Spatial and temporal Arctic Ocean depositional regimes: a key to the evolution of ice drift and current patterns, **Quaternary Science Reviews,** 29, 3644-3664, 2010.

[89] Stärz, M., Gong, X., Stein, R., Darby, D.A., Kauker, F., Lohmann, G.: Glacial shortcut of Arctic sea-ice transport, **Earth and Planetary Science Letters,** 357–358, 257–267, 2012.

[90] Stein, R., Grobe, H., Wahsner, M.: Organic carbon, carbonate, and clay mineral distributions in eastern central Arctic Ocean surface sediments, **Marine Geology,** 119, 269-285, 1994.

[91] Stein R.: Arctic Ocean Sediments: Processes, Proxies, and Paleoenvironment, **Elsevier,** Amsterdam, 1-592 pp, 2008.

[92] Stein, R., Matthiessen, J., Niessen, F.: Re-Coring at Ice Island T3 Site of Key Core FL-224 (Nautilus Basin, Amerasian Arctic): Sediment Characteristics and Stratigraphic Framework, **Polarforschung,** 79 (2), 81 – 96, 2010a.

[93] Stein, R., Matthiessen, J., Niessen, F., Krylov, A., Nam, S., Bazhenova, E., Shipboard Geology Group.: Towards a better (litho-) stratigraphy and reconstruction of Quaternary paleoenvironment in the Amerasian Basin (Arctic Ocean), **Polarforschung,** 79 (2), 97–121, 2010b.

[94] Stein, R., Fahl, K., Müller J.: Proxy Reconstruction of Cenozoic Arctic Ocean Sea-Ice History– from IRD to IP25, **Polarforschung,** 82 (1), 37–71, 2012.

[95] Stokes, C.R., Clark, C.D., Darby, D., Hodgson, D.A.: Late Pleistocene ice export events into the Arctic Ocean from the M'Clure Strait Ice Stream, Canadian Arctic Archipelago, **Global and Planetary Change,** 49, 139—162, 2005.

[96] Stokes, C.R., Clark, C.D., Storrar, R.: Major changes in ice stream dynamics during deglaciation of the north-western margin of the Laurentide Ice Sheet, **Quaternary Science Reviews,** 28, 721-738, 2009.

[97] Svendsen, J. I., Alexanderson, H., Astakhov, V. I., Demidov, I., Dowdeswell, J. A., Funder, S.,Gataullin, V., Henriksen, M., Hjort, C., Houmark-Nielsen, M., Hubberten, H. W., Ingólfsson, O., Jakobsson, M., Kjær, K. H., Larsen, E., Lokrantz, H., Lunkka, J. P., Lysså, A., Mangerud, J.,Matioushkov, A., Murray, A., Möller, P., Niessen, F., Nikolskaya, O., Polyak, L., Saarnisto, M., Siegert, R., Siegert, M. J., Spielhagen, R. F., Stein, R.: Late Quaternary ice sheet history of Northern Eurasia, **Quaternary Science Review,** 23, 1229–1271, 2004.

[98] Vogt, C.: Regional and temporal variations of mineral assemblages in Arctic Ocean sediments asclimatic indicator during glacial/interglacial changes, **Report on Polar Marine Research,** 251, 309, 1997.

[99] Vogt, C., Knies, J., Spielhagen, R. F., Stein, R.: Detailed mineralogical evidence for two nearly identical glacial/deglacial cycles and Atlantic water advection to the Arctic Ocean during the last 90,000 years, **Global and Planetary Change,** 31, 23–44, 2001.

[100] Vogt, C. and Knies, J.: Sediment dynamics in the Eurasian Arctic Ocean during the last deglaciation — The clay mineral group smectite perspective, **Marine Geology,** 250, 211–222, 2008.

[101] Vogt, C. and Knies, J.: Sediment pathways in the western Barents Sea inferred from clay mineral assemblages in surface sediments, **Norwegian Journal of Geology,** 89, 41–55, 2009.

[102] Viscosi-Shirley, C., Mammone, K., Pisias, N., Dymond, J.: Clay mineralogy and multi-element chemistry of surface sediments on the Siberian-Arctic shelf: Implications for sediment provenance and grain size sorting, **Continental Shelf Research,** 23, 1175–1200, 2003.

[103] Wahsner, M., Müller, C., Stein, R., Ivanov, G., Levitan, M., Shelekova, E., Tarasov, G.: Clay mineral distributions in surface sediments from the Central Arctic Ocean and the Eurasian continental margin as

indicator for source areas and transport pathways: a synthesis, **Boreas,** 28, 215-233, 1999.

[104] Wang, D. and Hesse, R.: Continental slope sedimentation adjacent to an ice-margin. II. Glaciomarine depositional facies on Labrador Slope and glacial cycles, **Marine Geology,** 135, 65-96, 1996.

[105] Wang, R., Xiao, W., März, C., Li, Q.: Late Quaternary paleoenvironmental changes revealed by multi-proxy records from the Chukchi Abyssal Plain, western Arctic Ocean, **Global and Planetary Change,** 108, 100–118, 2013.

[106] Winkler, A., Wolf-Welling, T.C.W., Stattegger, K., Thiede, J.: Clay mineral sedimentation in high northern latitude deep-sea basins since the Middle Miocene (ODP Leg 151, NAAG), **International Journal of Earth Sciences,** 91,133–148, 2002.

[107] Winter, B.L., Johnson, C.M., Clark, D.L.: Strontium, neodymium, and lead isotope variations of authigenic and silicate sediment components from the Late Cenozoic Arctic Ocean: implications for sediment provenance and the source of trace metals in seawater, **Geochimica et Cosmochimica Acta,** 61, 4181-4200, 1997.

[108] Xiao, W., Wang, R., Polyak, L., Astakhov, A., Cheng, X.: Stable oxygen and carbon isotopes in planktonic foraminifera *Neogloboquadrina pachyderma* in the Arctic Ocean: an overview of published and new surface-sediment data, **Marine Geology,** 352, 397-408, 2014.

[109] Xuan, C. and Channell, J.E.T.: Origin of apparent magnetic excursions in deep-sea sediments from Mendeleev-Alpha Ridge (Arctic Ocean), **Geochemistry, Geophysics, Geosystems,**11, Q02003, 2010.

[110] Yurco, L. N., Ortiz, J. D., Polyak, L., Darby, D. A., Crawford, K. A.: Clay mineral cycles identified by diffuse spectral reflectance in Quaternary sediments from the Northwind Ridge: implications for glacial–interglacial sedimentation patterns in the Arctic Ocean, **Polar Research**, 29, 176–197, 2010.

[111] Zou, H.: An X-ray diffraction approach: bulk mineral assemblages as provenance indicator of sediments from the Arctic Ocean, PhD Thesis, University of Bremen, Bremen, 1-104 pp, 2016.

Table 1. Minerals Actively Sought in Diffraction Data Analysis

Mineral	window(°2θ, CuKα radiation)	Range of D-Spacing(A)	Intensity Factor
Amphibole	10.30-10.70	8.59- 8.27	2.5
Augite	29.70-30.00	3.00- 2.98	5
Calcite	29.25-29.60	3.04- 3.01	1.65
Chlorite	18.50-19.10	4.79- 4.64	4.95
Dolomite	30.80-31.15	2.90- 2.87	1.53
K-Feldspar	27.35-27.79	3.26- 3.21	4.3
Quartz	26.45-26.95	3.37- 3.31	1

Table 2. AMS^{14}C datings in core BN05.

Sample no.	Depth (cm)	AMS 14C age (14C a BP)	Calibrated age median (cal yr BP)	2-σ range (cal yr BP)
112767	4-6	7810±35	7885	7797-7958
112768	8-10	8180±35	8259	8171-8340
112769	18-20	38600±300	41703	41202-42165
115944	22-24	40800±410	43140	42522-43901

1121 **Table 3.** Characterization and interpretation of ~~sedimentary~~ ~~variable~~ groups (Fig. 6)

1122

Group	**Leading**/ opposite proxies	Environments	Depositional processes	Provenance
1	**Foraminifers, calcite, Mn, clay**/ ~~coarse grains (esp. silt)~~, ~~quartz~~	Interglacial (incl. major interstadials)	Sea ice	Mixed
2	**Dolomite, Ca, Qua/Fsp** / ~~plagioclase, pyroxene, feldspar~~	Glacial/ deglacial	Icebergs, meltwater	North American
3	**Feldspar, pyroxene, plagioclase**/ ~~Ca, dolomite, Qua/Fsp~~	Interglacial/ deglacial	Sea ice, icebergs	Siberian
4	**Smectite, kaolinite, chlorite** / ~~clay~~	Glacial/ deglacial	Icebergs, debris flows	E Siberian
~~5~~, 6	~~**Coarse grains (incl. silt)**~~	Glacial/ deglacial	Icebergs, debris flows	Mixed

1123

1124

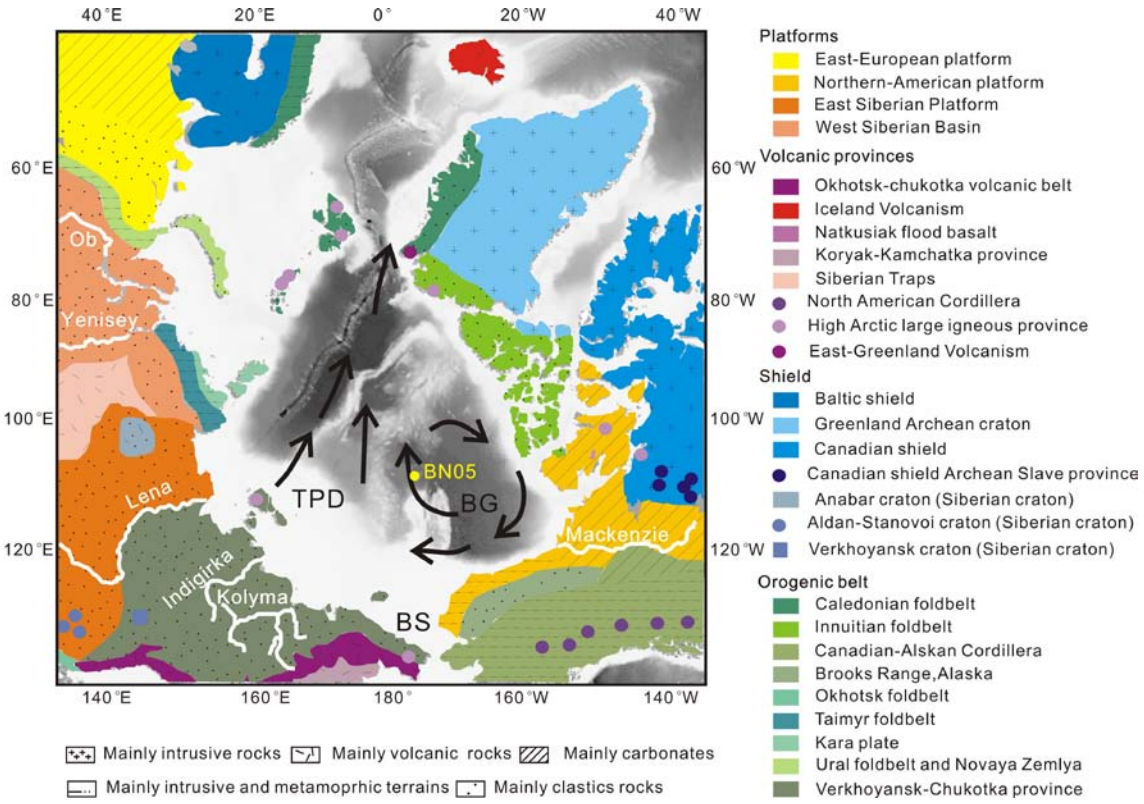

Figure 1. Background map showing the location of core ARC4-BN05, the main Arctic rivers and the two major surface current systems: Beaufort Gyre (BG) and Transpolar Drift (TPD). Schematic geological map shows the distribution and prevailing lithology of the main terrains adjacent to the Arctic Ocean (Fagel et al., 2014).

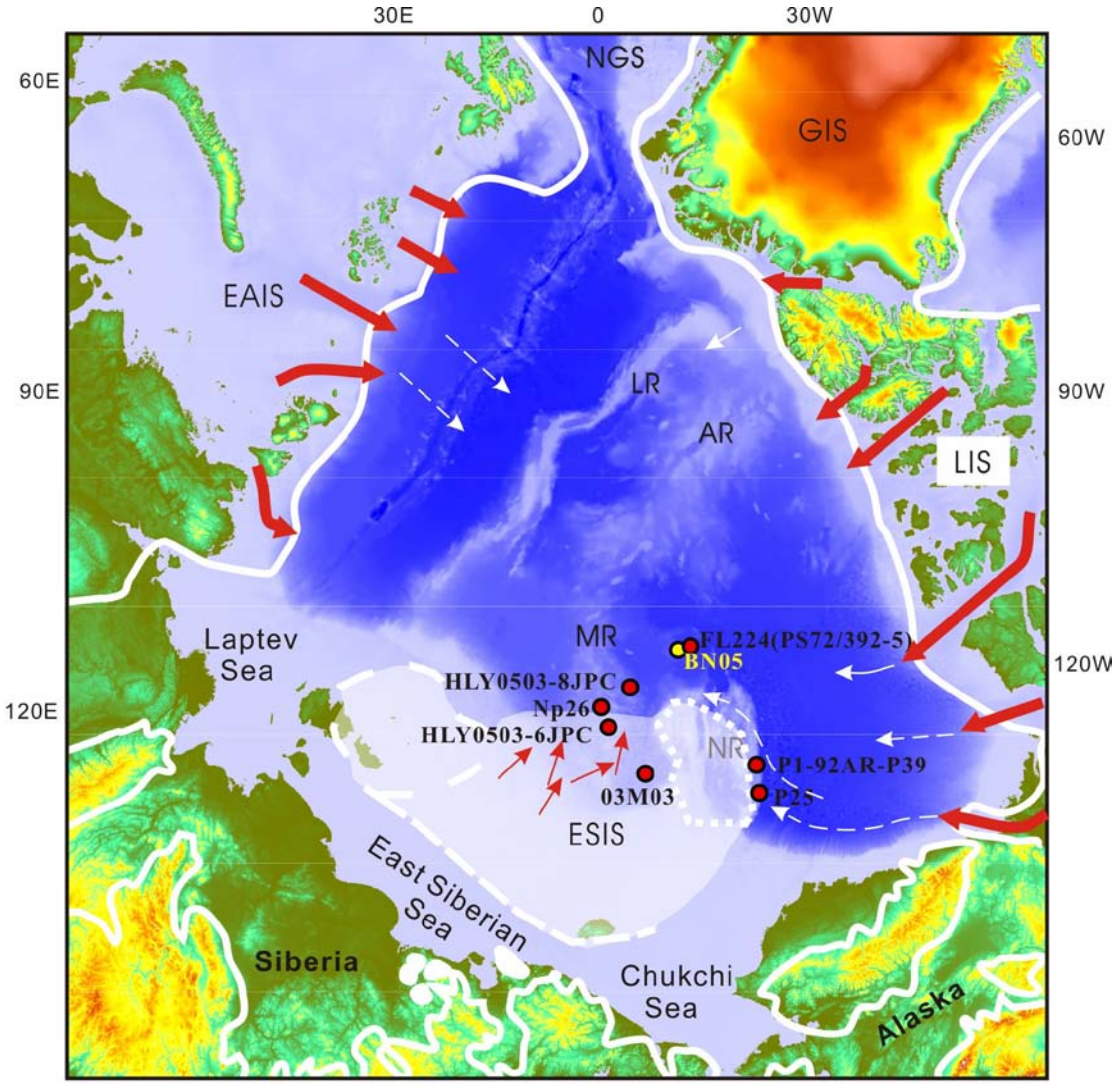

Figure 2. Index map showing the location of core ARC4-BN05 (yellow circle) and other cores from previous studies mentioned in this paper (red circles). LR, MR, AR, and NR are Lomonosov, Mendeleev, Alpha, and Northwind ridges, respectively; NGS is Norwegian–Greenland Sea. White lines show maximal Pleistocene limits reconstructed for Greenland, Laurentide, Eurasian, and East Siberian Ice Sheets (GIS, LIS, EAIS and ESIS; England et al., 2009; Svendsen et al., 2004; Niessen et al., 2013). Proposed flow lines for grounded ice sheets and ice shelves (red and white arrows, respectively) are after Niessen et al. (2013).

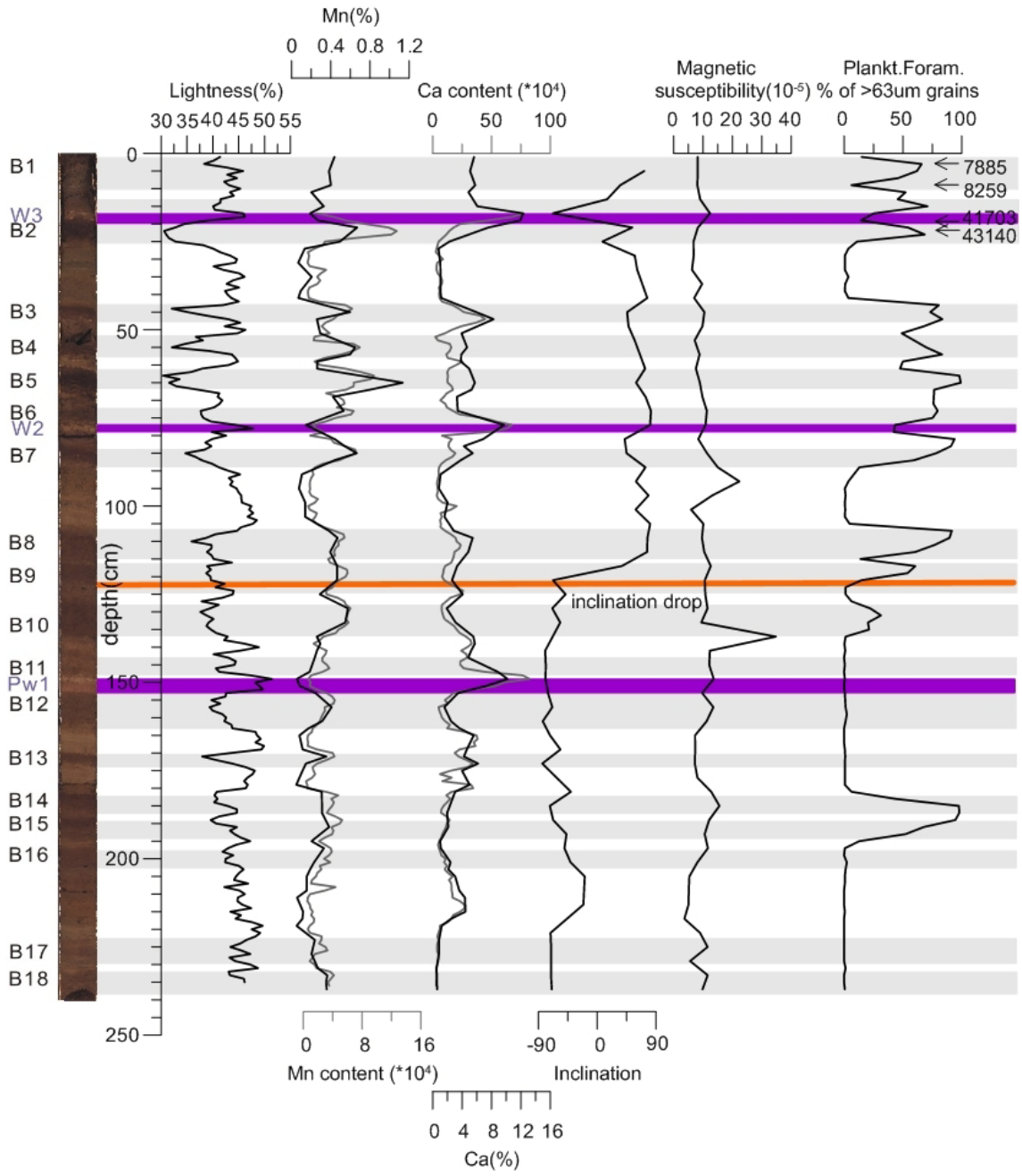

1143

1144 **Figure 3**. Lithostratigraphy and major proxies in core BN05: core photograph with

1145 brown layer indices, lightness, Ca and Mn content (bulk XRF –grey line, ICP-OES –

1146 black line), paleomagnetic inclination, planktic foraminiferal abundance, and AMS ^{14}C

1147 datings. Predominantly dark brown intervals B1-B18 are highlighted in grey; high-Ca,

1148 pink-white layers are marked by purple lines. The main inclination drop is marked by

1149 orange line. See Table S1 for data used.

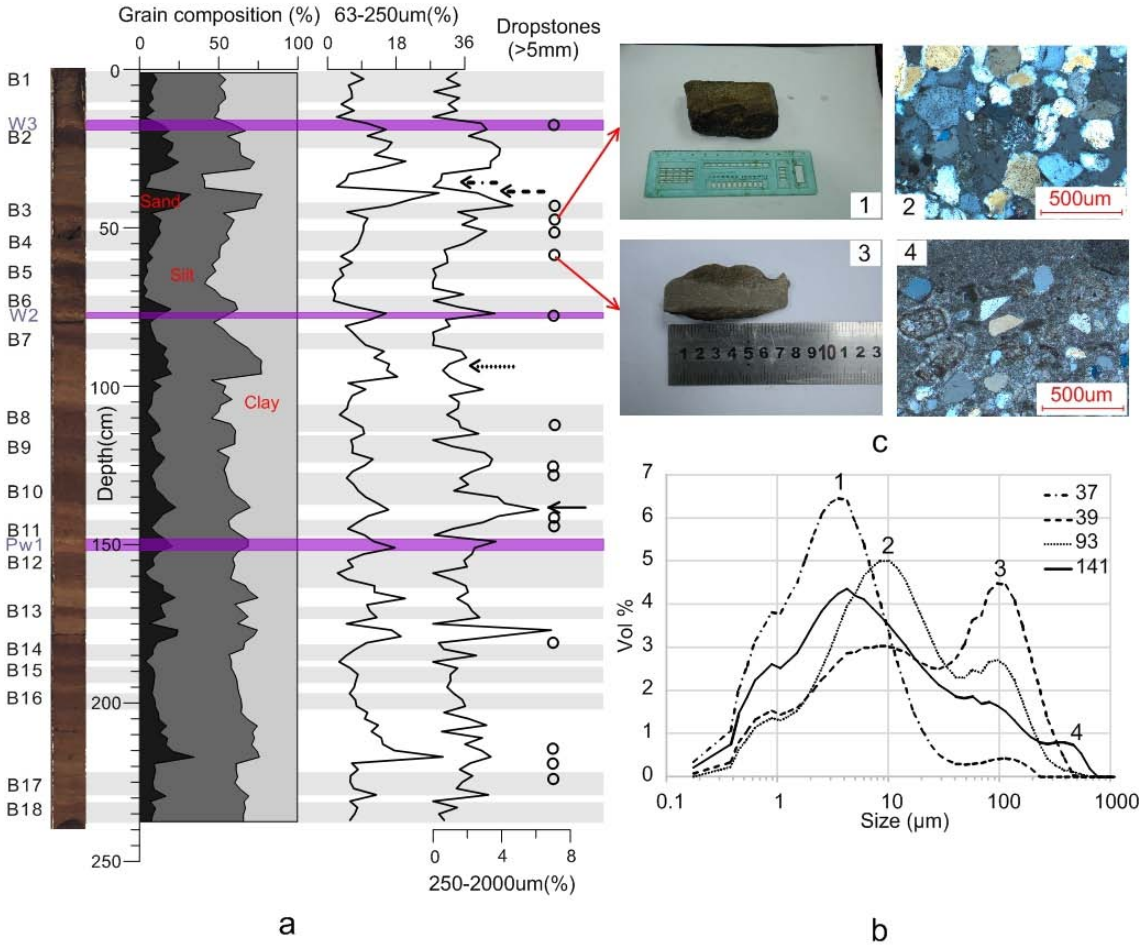

Figure 4. (a) Down-core grain-size distribution in core ARC4-BN05: clay (<4 μm), silt (4-63 μm), sand (63-2000 μm), fine sand (63-250 μm), and coarser sediment (250-2000μm). Occurrence of dropstones >5 mm is shown by circles on the right. See Fig. 3 for lithostratigraphy explanation, and Tables S1-2 for data used. **(b)** Granulometric distribution types exemplifying major grain-size modes 1-4. Position of respective curves in core ARC4-BN05 is indicated in the legend (depth in core, cm) and is shown by arrows in panel **a**. **(c)** Examples of dropstones from core ARC4-BN05. 1, 48-54 cm, quartz sandstone; 2, same dropstone, thin section in cross polarized light; 3, 56-63.5 cm, dolomite dropstone; 4, same dropstone, thin section in cross polarized light.

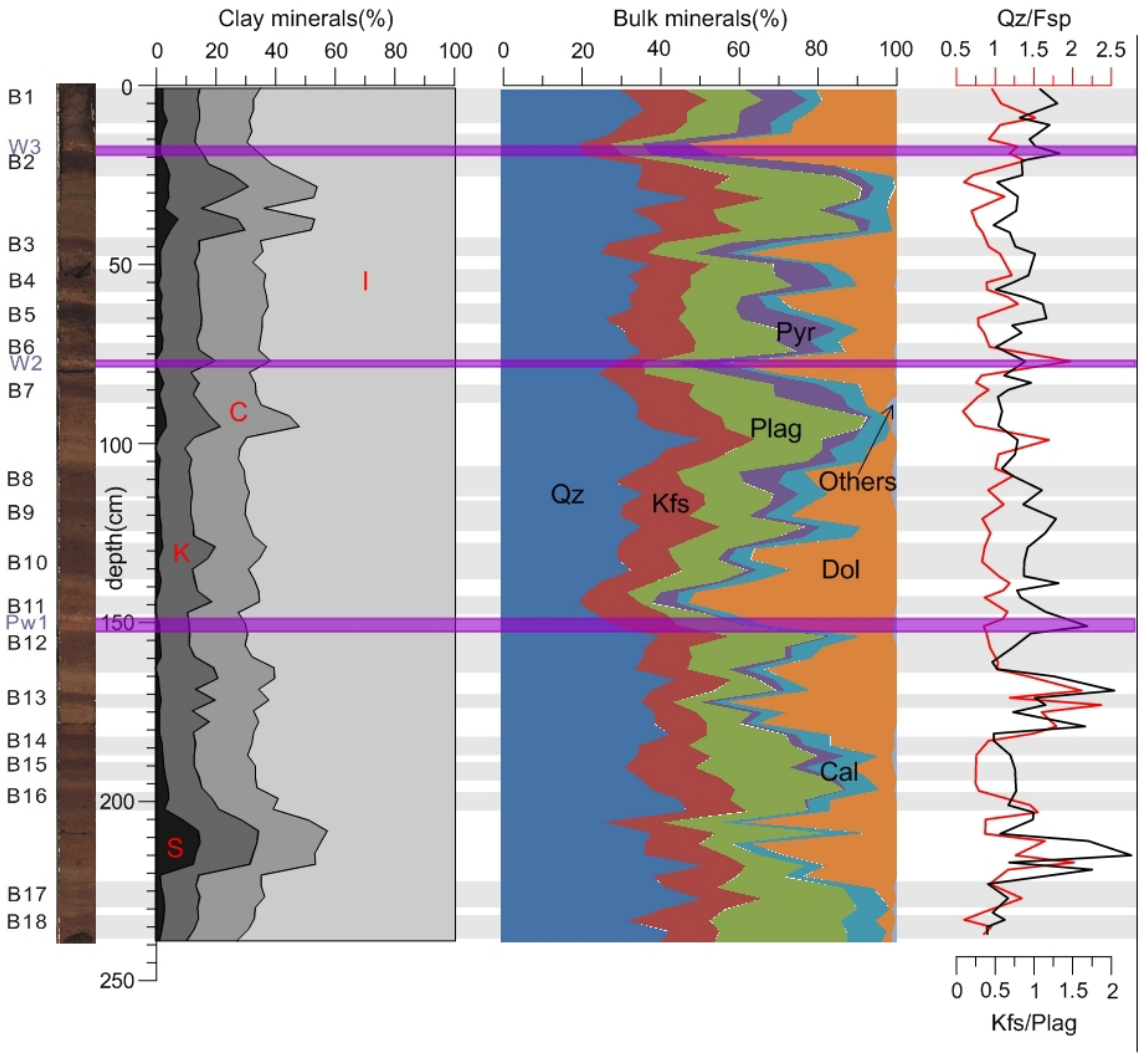

1162

1163 **Figure 5**. Relative weight contents of major clay mineral groups in the clay fraction

1164 (<2 μm), bulk mineral composition and related indices in core ARC4-BN05. S, K, C,

1165 and I indicate smectite, kaolinite, chlorite, and illite, respectively. Qz, Kfs, Plag, Pyr,

1166 Cal, and Dol are quartz, K-feldspar, plagioclase, pyroxene, calcite, and dolomite,

1167 respectively. See Fig. 3 for lithostratigraphy explanation and Table S1 for data used.

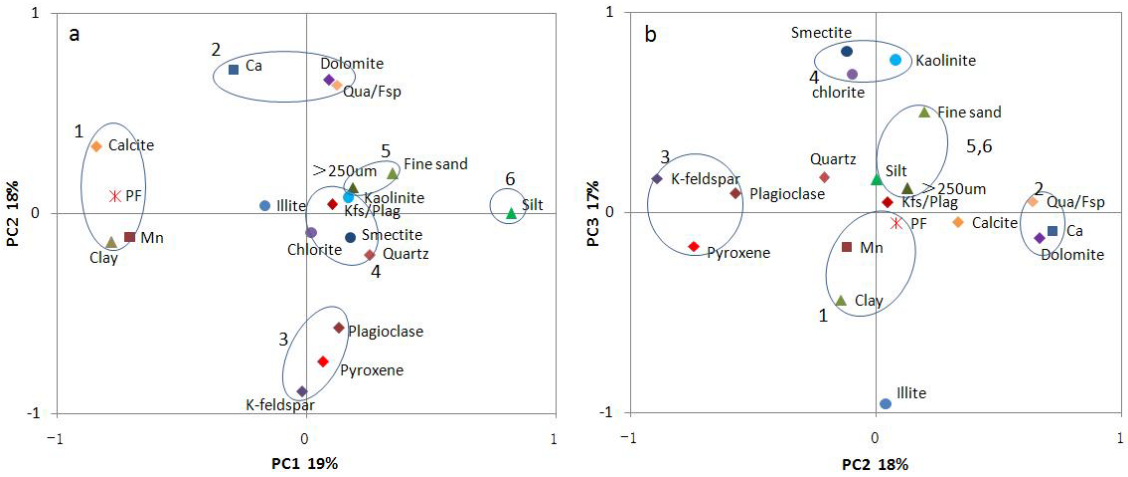

Figure 6. Biplots of Principal Component loading scores in PC 1-2 (a) and PC 2-3 (b) space. Sedimentary variable groups or end members revealed by the loading distribution are enclosed by ellipses and numbered (see Table 3 and text in section 5.2 for discussion). See Tables S3-4 for correlation between variables and PC loading scores.

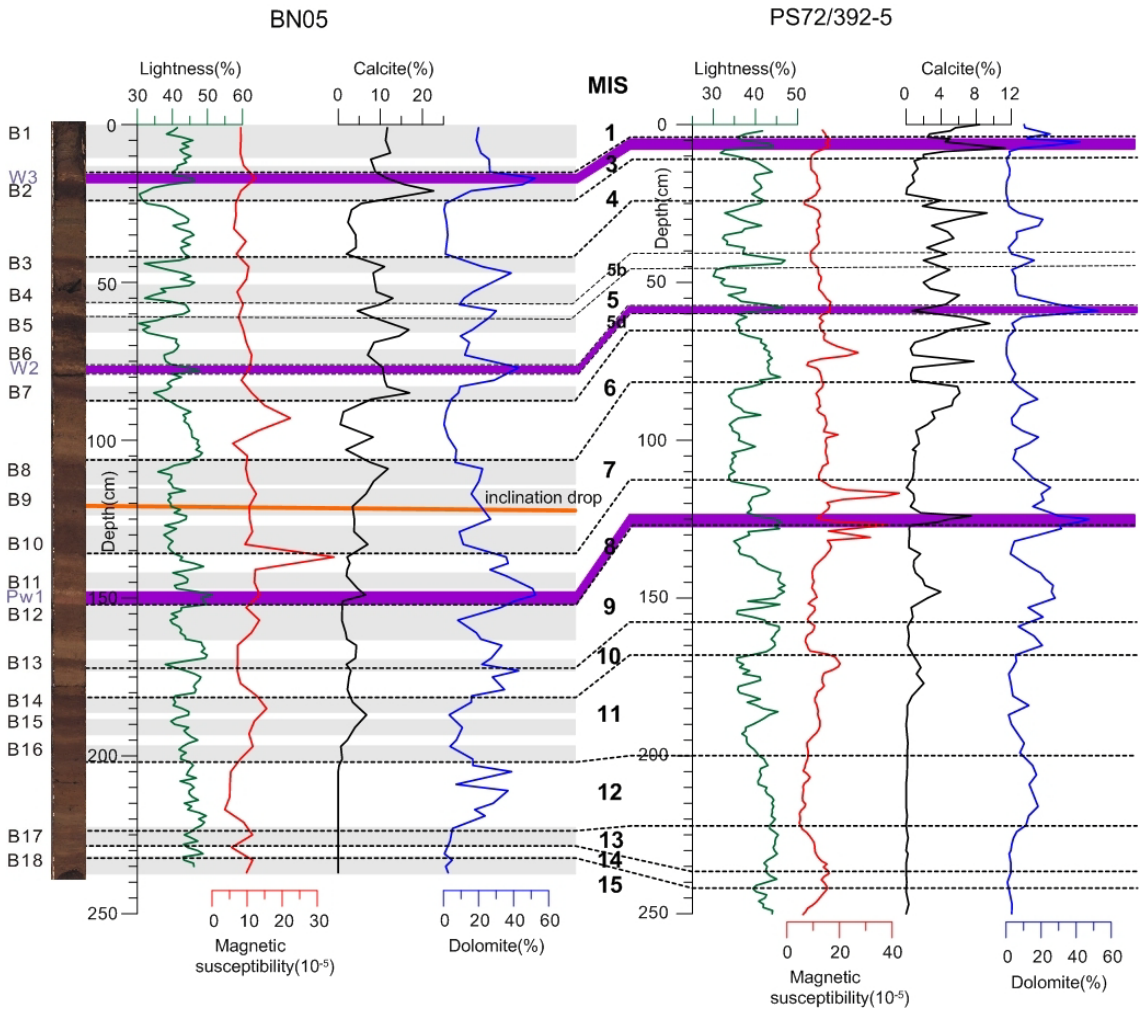

1174

1175 **Fig. 7**. Stratigraphic correlation of core BN05 with PS72/392-5 (Stein et al., 2010a)

1176 based on sediment lightness, magnetic susceptibility, calcite and dolomite content.

1177 See Fig. 3 for lithostratigraphy explanation.

1178

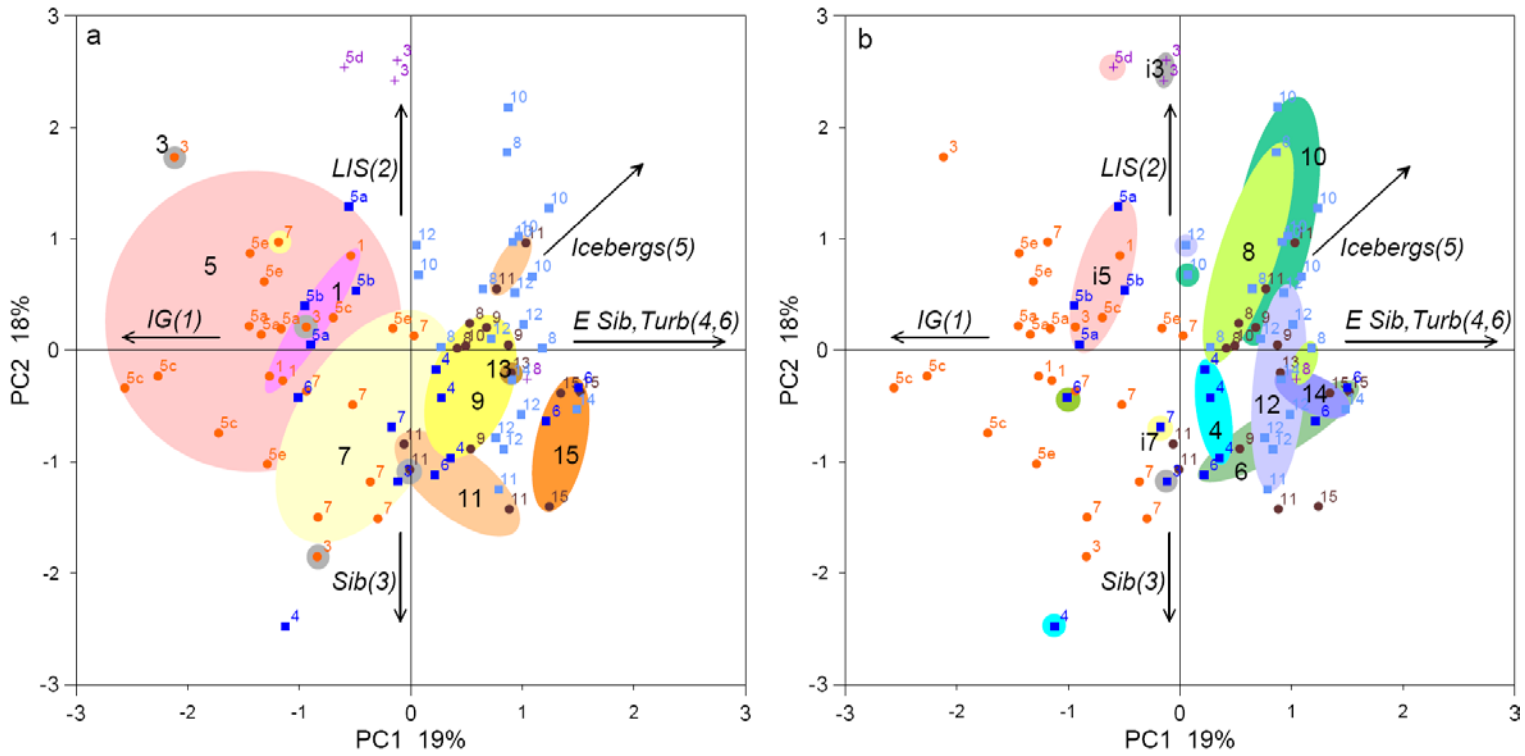

Figure 8. Biplots of downcore PC scores in the PC 1-2 space grouped by interglacial (a) and glacial intervals (b). Interpretation of loading score distribution: IG – interglacial environments, LIS – Laurentide Ice Sheet provenance, Sib/E Sib – Siberian/East Siberian provenance, Turb. – turbidites; variable group numbers shown in parentheses (Fig. 6; Table 3; see Section 5.2 above for more discussion). Numbers for individual and grouped samples show Marine Isotope Stages. See Table S5 for downcore PC score distribution.

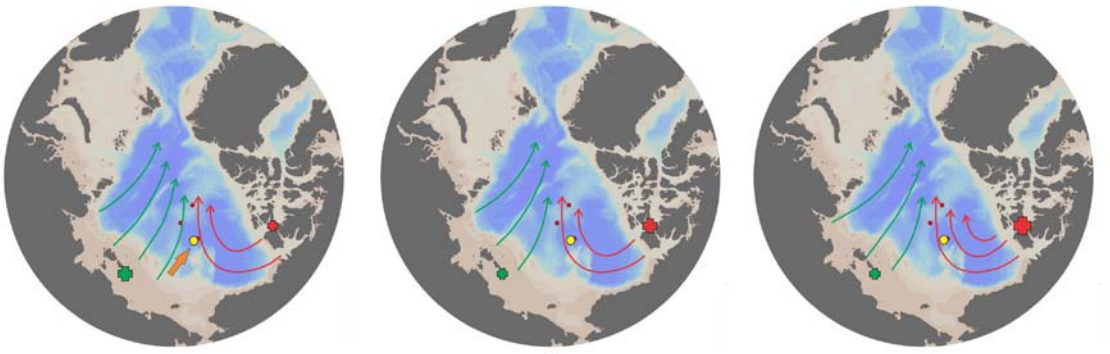

Figure 9. Schematic reconstruction of glacial environments in the western Arctic Ocean and factors controlling sedimentation at the BN05 site (yellow circle): surface circulation (red and green arrows), glacioturbidites (orange filled arrow), and ice-sheet size (red and green crosses). See Fig. 1 for modern circulation. (a) High ESIS inputs: MIS 4, 6, 12, and 14; (b) high LIS inputs: MIS 8 and 10; (c) especially high LIS inputs: intra-MIS5 and 3.